Article:

Wang, JP, Zeng, GH and Yu, HS orcid.org/0000-0003-3330-1531 (2019) A DEM investigation of water-bridged granular materials at the critical state. Computational Particle Mechanics, 6 (4). pp. 637-655. ISSN 2196-4378

https://doi.org/10.1007/s40571-019-00243-2

A DEM investigation of water bridged granular materials at the critical state

Ji-Peng Wang [a,*], Guo-Han Zeng [b] and Hai-Sui Yu [c]

[a] School of Civil Engineering, Shandong University, 17922 Jingshi Road, Jinan 250061, China
[b] Nottingham Centre for Geomechanics, Faculty of Engineering, University of Nottingham, University Park, Nottingham NG7 2RD, UK
[c] School of Civil Engineering, Faculty of Engineering, University of Leeds, Leeds LS2 9JT, UK

[*]. E-mail: Ji-Peng.Wang@outlook.com

Abstract

The critical state is an important concept for saturated and partially saturated granular materials as the strength and volume become constant and unique under continuous shear. By incorporating the water bridge effect, the mechanical behaviours of wet granular matters can be studied by the discrete element method (DEM). A series of DEM simulations are performed following the conventional triaxial loading path for dry and wet granular materials, and different suction values are applied at various confining stress levels. Unique critical state behaviours have been observed in both macroscopic and microscopic scales. It shows that the confining stress level plays an important role in the critical state behaviour of wet granular materials. The critical stress ratio for a wet material is not a constant value at different stress levels and it is found that both the critical stress ratio and void ratio in wet granular matters are also much higher with a low confining stress. A framework is proposed by considering both the contact stress and the capillary stress effects to model the critical state lines. At large strain, the coordination number, the mean inter-particle force and fabric anisotropies evolve to constant critical state values for both dry and wet materials. The macro parameters formulating the critical state stress ratio are found to be associated with the critical state anisotropies in solid skeleton and water phase fabrics respectively.

Keywords: wet granular material; critical state; micromechanics; discrete element modelling

1. Introduction

A granular material reaches the critical state as the shear strength and volume become stable when it is sheared to a relatively large deformation [27]. The critical state is independent of the initial void ratio and is generally regarded as a unique state. For partially saturated soils, the critical state also exists, and the critical state definition is used for modern constitutive modelling of unsaturated granular materials such soils [1, 13, 39, 40, 52].

Laboratory tests can be carried out to investigate the critical state of an unsaturated soil by maintaining constant suctions in the sample [41, 42, 51]. In laboratory tests, the water content is usually in relative high range due to the difficulty in applying higher suction. The critical state of unsaturated soils with relatively low water content, in which the water exits as discontinuous water bridges or absorption layers, have not been well understood. Moreover, in the recent development of soil mechanics, fabric and microstructure are usually regarded as important factors governing the macro behaviours [19]. The conventional laboratory tests may not provide the micro scale information.

The discrete element method (DEM) [8] is a discontinuous numerical method that can simulate granular matter as individual particles, and thus the contact force network and fabric can be obtained from the particle scale quantities. The DEM method can be employed to extend the classic experimental study on the critical state of granular materials, for example sands [2, 3, 15], to microscopic investigations. The micro characteristics of dry granular material at critical state are recently studied from aspects of fabric anisotropy, force transmission pattern and entropy convergence [14, 18, 37, 53, 54]. For wet granular materials, basic macroscopic features of the critical state behaviours have been observed in the context of rheological study [4, 16, 29]. However, a more systematic study of micromechanics of wet granular materials at the critical state, especially linking the macroscopic critical state behaviour to the micro structure evolutions, is still necessary.

Techniques for modelling wet granular materials in DEM are raised and developed in the last decade. The water phase and water-air interface effect are usually considered as water bridge effects between neighbouring grains [12, 26, 32, 34, 35, 38, 49] providing it has a low degree of saturation within the pendular state. Beyond the pendular state the water bridge may coalesce with each other [30, 46]. Although it is limited to low moisture content, simulations of these wet granular materials may still give evidence for the behaviours of unsaturated granular soils within a relatively low degree of saturation range, which is lack in laboratory studies.

In this study, a suction-controlled water bridge model [48] is employed to carry out a systematic study on the critical state behaviour of granular materials. Conventional triaxial loading path is applied to dense and loose specimens at different stress levels and various suctions. By decomposing the inter-particle force into a mechanical force and a capillary force, the total stress is then expressed as the sum of the mechanical contact stress and the capillary stress. The role of the contact stress in representing the effective stress at critical state is discussed. A framework is then proposed using the mean contact stress and the mean capillary stress to model the critical state stress ratio and void ratio. Based on the stress-force-fabric relationship for wet granular material [48], the connection between the critical state stress ratio and the internal fabrics of solid and water phases is investigated, mainly on the aspects of coordination numbers, mean force levels and also fabric anisotropies in solid and water phases. It should be noted that particle size distribution has a significant effect on the material hydraulic and strength properties [45, 47], whereas this study only focuses on one kind of grain size distribution and we leave the grain size distribution effect for future work.

2. DEM Simulation

2.1 Capillary bridge effect between particles

In this study, wet granular material behaviours are simulated by DEM with capillary bridge effect considered between neighbouring particles. The inter-particle force is the sum of the mechanical contact force and the capillary force on the water bridge when grains are in physical contact. When there is a distance between two grains but within the water bridge rupture distance, the inter-particle interaction is only raised by the capillary force (Fig. 1). Beyond the rupture distance, the inter-particle force vanishes.

For the capillary effect, suction is assumed to be constantly maintained throughout the material. By Young-Laplace equation, the geometry of the water bridge has the following relationship with suction as:

$$S = u_a - u_w = T\left(\frac{1}{r_{ext}} - \frac{1}{r_{int}}\right) \tag{1}$$

where S is the matric suction, u_a is the air pressure, u_w is the water pressure, T is the surface tension ($T = 0.073 N/m$) and r_{ext} and r_{int} are external and internal radius of the water bridge at the water bridge neck. In this study, the water bridge is simplified as toroidal shape (external radius is constant along the water bridge and the cross section is a circle). For a given pair of particles with known geometry (particle radius and inter-particle distance), suction (S), surface tension (T) and water-solid-air contact angle (θ), the shape of the water bridge (r_{ext} and r_{int}) can be obtained by an iteration method (more details can be seen in the previous work in [48]). The material is assumed to be hydrophilic and the water-solid-air contact angle is simplified as 0. With the obtained r_{ext} and r_{int}, the capillary force raised by the water bridge can be calculated by using the 'gorge method'. It is composed of two parts. One part is from the surface tension effect and another part is from the pressure difference (the suction) acting on the cross section of the bridge. Therefore, the capillary force can be calculated as:

$$f_{cap} = S\pi r_{int}^{2} + T(2\pi r_{int}) \tag{2}$$

The water bridge volume can be obtained from the integration of the water bridge profile with the part of the grain subtracted. The water bridge model is incorporated into the classical Hertz-Mindlin contact model in DEM simulations. In this study, the open source DEM platform LIGGGHTS [17] is employed for its easier access to the source code and applicability on high-performance computing service.

2.2 Sample preparation and water retention curve

The behaviours of dry and wet granular materials are investigated by a representative volume element (RVE). The tested samples are made of spherical particles with a cubic shape upon generation confined by smooth rigid wall boundaries. Particle diameters are uniformly distributed from 0.018mm to 0.022mm and the initial length of the RVE is 0.4mm (20 times of mean grain size and the total grain number is around 9000). The contact model for the solid contacts is the typical Hertz model. The material property parameters of the particles are based on the typical quartz material. The material density of grains is 2500 kg/m^3. Young's modulus and Poisson's ratio of the particles are 70GPa and 0.25 respectively. The inter-particle friction coefficient is 0.5, which is a typical value for quartz sand. The coefficient of restitution, which is defined as the ratio of the final to initial relative velocity between two particles after a collision, is 0.2. Therefore, the coefficient of restitution is a parameter governing the energy dissipation process in the system.

The specimens are prepared by using the radius expansion method without capillary effect. Particles with reduced sizes are firstly inserted without any contact in the cubic mould. Then, radii of the particles are increased gradually to the target size. Two samples with different initial void ratio values (e=0.629 and e=0.732) are firstly prepared at 10kPa confinement. The two samples are then compressed isotropically to different mean stress levels. The isotropic normal consolidation lines (noted as INCL) of these two specimens can be seen in Fig. 2 (in lines) where p is the mean normal stress as:

$$\mathrm{p} = \frac{\sigma_1 + \sigma_2 + \sigma_3}{3} \tag{3}$$

The wet specimens are prepared based on the dry materials at the corresponding mean normal stress levels (at 10kPa, 20kPa, 50kPa, 100kPa, 200kPa, 500kPa, 1MPa, 2Mpa and 10MPa). Capillary bridge effect is applied to particle pairs within the rupture criteria. As the capillary force is an attractive force, the material is further consolidated by maintaining the total boundary stress. The wet specimens at $S = 20kPa$ are also presented in Fig. 2 (in symbols). It can be seen that the wetting process doesn't have an obvious effect on the void ratio.

By summing the water bridge volume and dividing by the void volume, degree of saturation of a specimen at a certain suction value can be calculated. The relationship between the degree of saturation (S_r) and suction is generally named as the water retention curve. Fig. 3 depicts the void ratio and mean normal stress effect on the water retention curve within the pendular state (the water bridge model is not valid for higher water content conditions). Under 10kPa mean stress, the dense sample has a higher degree of saturation at the same suction. It can also be observed that increasing the mean normal stress to 2MPa does not obviously alter the water retention behaviour.

2.3 Triaxial shearing to the critical state

After the preparation of isotropic specimens, conventional triaxial loading path is applied to shear the samples to the critical state. The horizontal confining stresses ($\sigma_2 = \sigma_3$) are maintained at a constant value and the axial strain (ε_1) is applied by moving the boundaries in the axial direction. Fig. 4 is a sketch of the loading path in which the deviatoric stress is:

$$q = \sigma_1 - \sigma_3 \tag{4}$$

The triaxial deformation satisfies the quasi-static condition. The quantity of unbalanced force ratio, which is the ratio between average unbalanced force on grains and mean interparticle forces, is adopted to certify the quasi-static condition. During the triaxial test, the unbalanced force ratio is controlled to be less than 0.01 by adjusting the axial strain rate.

The critical state means that the shear strength and void ratio are constant when the material is sheared to a certain deformation and the final shear strength and void ratio are independent of the material initial state. Typical behaviours of dry and wet materials (at 20kPa suction) with 10kPa confining stress in triaxial loading are presented as an example. In Fig. 5, the evolution of the total deviatoric stress (q), deviatoric and mean stresses in mechanical contact stress component (q_{cont} and p_{cont}), volumetric strain (ε_v), void ratio (e) and degree of saturation (S_r) of the dense and loose samples are depicted. All the variables become nearly constant when the samples are sheared to 0.4 strain. It should also be noted that it has also been observed by other authors that the granular material reaches the critical state around 0.4 axial strain by DEM simulation [53]. In Fig. 5a, the capillary effect significantly increases the material deviatoric stress. For both dry and wet materials, there is a unique ultimate deviatoric stress regardless the initial void ratio difference. For the volumetric strain behaviour in Fig. 5b, the capillary effect significantly enlarges the dilatancy which leads the ultimate volumetric strain of wet materials to be much higher. Correspondingly, the void ratio evolution during triaxial shearing is presented in Fig. 5c. Both dry and wet materials reach a unique void ratio. As the capillary force is cohesive that a wet granular material can afford larger voids upon loading, the critical state void ratio for wet granular materials at 10kPa confining stress is obviously larger. Furthermore, although the initial degree of saturation is different for dense and loose specimens, it is observed that there should be a same critical state degree of saturation (Fig. 5d), which could be related to the critical state void ratio.

Similar triaxial tests are then implemented on both dense and loose specimens at various confining stresses and suctions. Table 1 is a summary of the parameters for the triaxial tests carried out in this study. For each pair of suction and confining stress, both the loose and dense specimens prepared from the normal consolidation process in Fig. 2 are tested. All samples are sheared to 0.4 axial strain and the final stage is regarded as the critical state. The critical state values on both the macro and micro behaviours (taking the average value of the dense and loose samples) can then be employed for further investigations in the following sections.

3. The Critical State Behaviour

3.1 Contact stress and effective stress

In classic critical state soil mechanics [31], formulating the critical state line (CSL) requires descriptions of the deviatoric stress and void ratio by the mean stress (or mean effective stress). For dry (or fully saturated) granular materials, critical state deviatoric stress can be expressed as:

$$q = Mp' \tag{5}$$

where p' is the effective mean stress and M is the critical state stress ratio (slope of CSL in $p - q$ space). According to Li et al. [20], for granular materials, the specific volume, as $\nu = 1 + e$ (e is the void ratio), has the following relationship with mean effective stress:

$$\nu = 1 + e = \Gamma - \lambda \left(\frac{p'}{p_a} \right)^{\xi} \tag{6}$$

where Γ is a parameter denoting ν at $p' = 0$, λ and ξ are material parameters and p_a is the atmosphere pressure (101kpa).

The effective stress for unsaturated granular materials is still a controversial definition. The net stress $(\sigma - u_a)$ and suction $(u_a - u_w)$ are widely accepted as the two variables that should be used in the effective stress definition. The classic Bishop's effective stress [5] is expressed as:

$$\sigma'_{ij} = \left(\sigma_{ij} - u_a\right) + \chi\left(u_a - u_w\right)\delta_{ij} \tag{7}$$

where δ_{ij} is the Kronecker delta and χ is a parameter related with the degree of saturation. After Lu's suction stress definition [22], the χ parameter may be approximated as the degree of saturation or the effective degree of saturation. In this numerical study, as the absorption layers are not considered, the macroscopic effective stress may be expressed as:

$$\sigma'_{ij} = \left(\sigma_{ij} - u_a\right) + S_r\left(u_a - u_w\right)\delta_{ij} \tag{8}$$

One of the benefits to study unsaturated granular materials using DEM method is the possibility to obtain the microscopic stress expression from grain scale interactions. With capillary bridge effects, the inter-particle force is composed of the mechanical contact force and the capillary force. Thus, the total stress tensor can be decomposed into a contact stress tensor (σ_{ij}^{cont}) counting only the mechanical contact force and a capillary stress tensor (σ_{ij}^{cap}) raised from capillary forces [33, 48]. With the aid of

DEM simulation, by applying the homogenisation technique [7] and following the expressions in [33, 48], the stress tensor can be calculated from particle scale interactions as:

$$\sigma_{ij} = \sigma_{ij}^{cont} + \sigma_{ij}^{cap} = \frac{1}{V}\sum_{s\in V} v_{cont\,i}^{\ s} f_{cont\,j}^{\ s} + \frac{1}{V}\sum_{w\in V} v_{cap\,i}^{\ w} f_{cap\,j}^{\ w} \tag{9}$$

where s and w denote the s-th inter-particle solid contact and the w-th water–particle interaction respectively (the total number is not necessarily the same). ${v_{cont}}_i^s$ is the contact vector pointing from the s-th contact point to the particle centre and ${v_{cap}}_i^w$ is a vector from the water bridge centre to the particle centre. ${f_{cont}}_i^s$ and ${f_{cap}}_i^w$ are the corresponding contact force and capillary force associated with the defined vectors. The positive direction of a force is defined from the interaction point to the particle; therefore, the attractive capillary force is a negative force leading the capillary stress tensor always to be negative. It should also be noted that the frictional force is part of the contact force. Therefore, the contact force is not necessarily to be normal to the particle.

The micromechanical stress tensors are usually employed in the study of granular material behaviours in both dry and partially saturated states. Some researchers attempted to describe the shear strength criteria of wet granular materials by using the contact stress tensor [10, 32, 43]. However, it has also been argued by some authors that using the contact stress is not adequate to model the material deformation [6, 11]. Here, the authors verified this again at the critical state by using the contact stress tensor to formulate the deviatoric stress and void ratio.

Firstly, the critical state deviatoric stress is investigated at different mean stress levels. Fig. 6a shows the relationship between the critical state deviatoric stress and the mean stress at various suctions. For a clearer presentation, only low stress states ($p < 150kPa$) are plotted. It can be seen that for the dry granular matter there is a linear $p - q$ relationship as Eq. 5. For unsaturated materials, due to the capillary effect, the critical state deviatoric stress is higher than that of the dry material. In Fig. 6b, the $p' - q$ relationship is presented, where p' is the mean effective stress and $q = q'$ as the suction induced stress is assumed to be isotropic in Eq. 8. However, as it can be seen in Fig. 6b, by using the effective stress definition in Eq. 8, the points don’t fall in the same line. This is because of, in reality, when the water content is relatively low, the suction induced stress may not be isotropic. It can also be seen in Fig. 6c in which the critical state deviatoric stress is plotted in the $p_{cont} - q$ space ($p_{cont} = \frac{\sigma_1^{cont}+\sigma_2^{cont}+\sigma_3^{cont}}{3}$). Using p_{cont} as the effective stress will also overestimate the deviatoric stress for wet materials as the CSL is almost above the simulated data points. This is because the capillary stress has been proven to be an anisotropic stress tensor associated with the solid structure anisotropy [32, 48, 50]. In Fig. 6d, the relationship between contact deviatoric stress $q_{cont} = \sigma_1^{cont} - \sigma_3^{cont}$ and mean contact stress p_{cont} is investigated. It looks like that the $p_{cont} - q_{cont}$ relationship for various suctions nearly fall in a linear line, which is also the conclusion drawn in [10, 32, 43] for the $p_{cont} - q_{cont}$ relationship but at the peak strength. The coefficient of determination (R^2 value) also proves that in the $p_{cont} - q_{cont}$ space the united critical state line has the best fitness.

We may further investigate the critical state void ratio to validate if the contact stress can be adequately used as the effective stress in deformation. The relationship between critical state void ratio and p_{cont} is demonstrated in Fig. 7. For the dry material, the $p - e$ relationship can be fitted by Eq. 6, in which ξ is simplified as 1, $\Gamma = 1.755$ and $\lambda = 9.89 \times 10^{-5}$. Due to the higher dilatancy in wet granular media, the critical state void ratio is obviously higher than that of the dry material, especially when the mean contact stress is relatively low. This indicates that using the contact stress tensor as the 'effective stress' is not enough, especially for modelling low stress conditions. A more complex relationship for the CSL is required that involves both the capillary stress and the contact stress.

3.2 Critical state formulation

Besides using an effective stress definition to model the critical state behaviour for unsaturated soils, based on laboratory experiments, Toll [40–42] proposed a framework for the unsaturated soil critical state using two stress state variables: the mean net stress $(p - u_a)$ and suction $(u_a - u_w)$. It can overcome the difficulty in modelling stress ratio and void ratio. In this framework, the deviatoric stress at the critical state is modelled as:

$$q = M_a \left(p - u_a \right) + M_b \left(u_a - u_w \right) \tag{10}$$

where the parameter M_a denotes the contribution of the mean net stress on the stress ratio and the parameter M_b represents the effect of suction on total stress ratio. Similarly, the specific volume (and void ratio) at critical state is written as:

$$\nu = e + 1 = \Gamma_a - \lambda_a \ln\left(p - u_a \right) - \lambda_b \ln\left(u_a - u_w \right) \tag{11}$$

where Γ_a represents the specific volume when both $p - u_a$ and $u_a - u_w$ are 1kPa and λ_a and λ_b are parameters associated with effect of $p - u_a$ and $u_a - u_w$ respectively.

In laboratory experiments, only the macro state variables ($p - u_a$ and $u_a - u_w$) can be measured. By using DEM, the stress tensor of a wet granular material can be expressed as Eq. 9. Thus, the contact stress (p_{cont}), which is the physical mechanical stress transmitting through solid contacts, and the capillary stress raised by water meniscus can be used to model the critical state framework. The capillary stress can also be expressed by contact stress and total stress as: $p_{cap} = p - p_{cont}$. Similar to Eq. 10, the deviatoric stress could be modelled as:

$$q = M_s p_{cont} + M_w \left(p - p_{cont} \right) \tag{12}$$

where M_s and M_w are model parameters representing the stress ratio contributed by the mean contact stress and mean capillary stress respectively. Thus the critical state stress ratio is:

$$M = \frac{q}{p} = M_s \frac{p_{cont}}{p} + M_w \frac{p - p_{cont}}{p} \tag{13}$$

It can be seen that when it is absolutely dry or fully saturated, $p = p_{cont}$, then $M = q/p = M_s$. Moreover, when the mean stress is relatively high, the effect from the capillary stress is also smaller to the total stress ratio. In addition to the soil mechanics point of view, Roy et al. [29] proposed another relationship between cohesion effect and critical state stress ratio based on the definition of bond number of the specimen, expressed as $Bo = \frac{f_{cap}^{max}}{p\bar{d}^2}$, in which f_{cap}^{max} is the maximum capillary in the specimen and $\bar{d}$ is the mean grain diameter. In their study, bond number has a linear relationship with critical state stress ratio. Similarly, we plot the relationship between bond number and critical state stress ratio in Fig. 9. The linear relationship is consistent with the previous study and the relationship can be fitted as:

$$M = \alpha_w Bo + M_s \tag{14}$$

where M_s is the critical state stress ratio for dry granular materials and α_w is the slope the linear relationship which is related to suction.

For the void ratio at the critical state, the formula can be extended from Eq. 6. It has been observed by [36] by using DEM method that there is a linear relationship between solid fraction $(\frac{1}{1+e})$ and mean pressure for cohesionless granular materials at the critical state. Therefore, $\xi = 1$ is taken in this study to represent the linear relationship between pressure and void ratio. In Fig. 7, critical state void ratio for wet granular materials is higher than that of the dry material, however, when the mean stress level is higher, the difference is reduced. Therefore, we propose the following equation to model the specific volume.

$$\nu = e + 1 = \Gamma_s - \lambda_s \left(\frac{p_{cont}}{p_a} \right) - \lambda_w \left(\frac{p - p_{cont}}{p} \right) \tag{15}$$

where Γ_s is the specific volume of a dry material when $p = 0kPa$, p_a is the atmosphere pressure as 101kPa, λ_s and λ_w are material parameters. In this equation, the capillary stress effect is presented by $\frac{p-p_{cont}}{p}$ in which the effect of p is considered. This means that when the mean stress is very large, the effect of the capillary stress on void ratio becomes less significant. The suction/capillary cohesion increased the critical state void ratio in Fig. 7 and Fig. 10, especially for low stress conditions. This is consistent with the work done by Roy et al. [29] , in which the volume fraction (void ratio) is increased with bond number (a relative measurement of cohesive effect), although the shape of the sheared specimen is different. This is because the cohesive force between particles leads to particle granulation, which can support larger inter-particle space especially in the sheared zones.

3.3 Critical state lines and parameters

Based on the proposed critical state framework based on the view of soil mechanics, the critical state lines on stress ratio, deviatoric stress and void ratio are investigated at various suction values. In Fig. 8, the critical state lines are depicted in the $p-M$ space and the $p-q$ space respectively. In the $p-M$ space, the dry material critical state stress ratio is around 0.73 and it is not obviously affected by mean stress. The value is consistent with the result in another DEM simulation [37] in which the inter-particle friction coefficient is also 0.5. However, the critical state stress ratios for wet granular materials are not constant values in different mean stress levels, they are higher than the dry material value at low stress conditions due to the capillary effect. The capillary effect on stress ratio decreases with the increase of mean stress level. This is because of that the capillary effect is almost independent of the mean stress level and the contribution of capillary stress on stress ratio is more significant at relatively low stress conditions. At high stress levels all critical state stress ratio values of wet materials converge to the dry material critical state stress ratio value. The results of the proposed critical state framework (Eq. 13) are plotted in lines. At high stress levels, the stress ratio is mainly contributed by the contact stress tensor and the total stress ratio values are similar. Considering the above fact, the parameter M_s for the dry material as 0.73 is used for all dry and wet materials. The parameter M_w represents the effect of capillary stress and is fitted for different suctions. The $p-q$ space critical state lines are presented in Fig. 8b. As the mean capillary stress is almost constant for different mean total stress levels, the critical state lines in high stress range are almost the same. A clearer presentation of the capillary effect on critical state shear strength can be seen in the inset in which the mean stress is lower than 100kPa. This also indicates that the water effect on strength is more important for low mean stress conditions.

Similarly, the critical state lines in the $p-$e space are then presented in Fig. 10. The results of Eq. 15 are in solid lines with points as the measured values. The parameters of Γ_s and λ_s are taken from the dry material results and not altered by suction. The parameter λ_w is fitted for different suctions. As $S = 5MPa$ presents a condition that the material has a very low degree of saturation ($S_r < 0.001\%$), this indicates that a small amount of water will increase the material's dilatancy and void ratio at the critical state significantly in the low mean stress state. However, further change in suction (thus water content) does not alter the void ratio obviously. It also shows that with the increase of mean stress level, the discrepancies in critical state void ratio between the dry and wet materials are reduced. The $p-$e lines for wet materials converge to the dry state line at high stress.

Fig. 8 and Fig. 10 only present part of the simulated results to have more explicit plots. Table 2 gives a summary of critical state parameters of all simulations in Table 1. As introduced in Fig. 5d, when the unsaturated material reached the critical state, there is a unique degree of saturation. The relationship between critical state stress ratio parameters and degree of saturation from the DEM simulation results are demonstrated in Fig. 11a. In the dry state, we define that $M_s = M_w = 0.73$. Although M_w has no true meaning at the dry state, this is to imply that when the water content is extremely low, the water bridges should share the same directional distribution with the inter-particle contacts. With a very small amount of water added in the material, M_w reduces significantly to around 0.2 and further increase of degree of saturation from 4% to 10% has little influence on M_w. In this study, the water bridge model is only valid within the pendular state. With the recent developments of other numerical method, such as coupling granular matter with the Lattice Boltzmann method in [9, 25], the capillary stress and thus the contact stress can be calculated. Using contact stress to model the critical state can be expected to be applied to the funicular and capillary states in the near future. Beyond the pendular state, we may imagine that the water bridges start coalesced and the capillary effect will be gradually reduced. When it is fully saturated, $u_a - u_w = 0$ and $p_{cap} = 0$. In Eq. 12, the capillary stress is related to suction. Therefore, one possible trend of M_w is that it increases in the funicular state and reaches to value of M_s at fully saturation. Another possibility is that M_w converges to 0 at saturation (Fig. 11b). This is from the implication that the capillary stress tensor could become a rather isotropic tensor with a high water content. This will be investigated in the next section. Moreover, the relationship between degree of saturation and parameter λ_w is presented in Fig. 12. It can be seen that λ_w varies around 0.04 and the water content effect on λ_w is not obvious.

4. Micro-characteristics at the Critical State

4.1 General relationship between stress state and microstructures

After the pioneering work of [21, 28], the stress tensor of a granular material is intrinsically related to its fabric and mean interparticle force, which is known by the stress-force-fabric relationship. The statistical micro interpretation of stress of wet granular materials can also be seen in [24] based on two dimensional simulations in which the repulsive contact force and attractive capillary force were integrated together as ‘bond forces’. In their work, the critical stress ratio can be expressed as the anisotropies of different micro-scale based quantities. In addition to this earlier work, a stress-force-fabric relationship for wet granular materials was developed by our previous work [48] to have an explicit understanding of the connection between the macro stress and the micro fabrics and forces associated with the contact stress and capillary stress respectively. It should be noted here that the capillary force does not necessarily act on a physical inter-particle contact, as the capillary bridge can be formed between neighbouring particles with a small gap less than the water bridge rupture distance. In this case, the capillary stress effect may be less anisotropic upon loading than that of the contact stress and it is necessary to study the stress tensors separately.

In our interpretation, for a representative elementary volume V with N particles inside, the total stress tensor, as a sum of the contact stress tensor and the capillary stress tensor, can be approximated by its internal fabrics and forces as:

$$\sigma_{\mathrm{ij}} \approx \frac{\mathrm{N}\overline{\mathrm{R}}}{3\mathrm{V}} \omega_{\mathrm{s}}\, \mathrm{f}_{\mathrm{cont}0} (\delta_{\mathrm{ij}} + \mathrm{G}^{\mathrm{sf}}_{\mathrm{ij}} + \frac{2}{5}\mathrm{D}^{\mathrm{s}}_{\mathrm{ij}} + \frac{2}{5}\mathrm{D}^{\mathrm{s}}_{\mathrm{im}_1}\mathrm{G}^{\mathrm{sf}}_{\mathrm{jm}_1}) + \frac{\mathrm{N}\overline{\mathrm{R}}}{3\mathrm{V}} \omega_{\mathrm{w}}\, \mathrm{f}_{\mathrm{cap}0} (\delta_{\mathrm{ij}} + \frac{2}{5}\mathrm{D}^{\mathrm{w}}_{\mathrm{ij}}) \qquad (16)$$

where $\bar{R}$ is the mean particle radius, ω_s is the solid contact coordination number (average physical contacts per particle), ω_w is the water bridge coordination number (average solid-water interactions per particle, normally $\omega_w \neq \omega_s$), ${f_{cont}}_0$ and ${f_{cap}}_0$ are parameters quantifying the directional mean contact and capillary forces respectively. The tensors in the equation, D_{ij}^s, D_{ij}^w and G_{ij}^{sf}, are obtained from the directional distributions of solid contact normals, water bridge directions and solid contact forces respectively. More details about this relationship can be referred to [48] and a reintroduction about procedures to calculate the three direction tensors can also be seen in the appendix after this paper.

The evolutions of the micro parameters during the triaxial shearing are then studied. The evolutions of the micro parameters for the set of tests in Fig. 5 (dry and wet granular materials are sheared at 10kPa confining stress) are presented as examples in Fig. 13. The evolutions of coordination numbers of solid contacts and water-solid interactions (ω_s and ω_w) for the dry and wet granular materials ($S = 20kPa$) are depicted. In Fig. 13a, the solid contact coordination numbers are higher in the wet granular material due to the attractive capillary force. Independent to the initial number, by shearing the material to large deformation, there are unique critical state solid coordination numbers for dry and wet materials respectively. In wet granular materials, the water bridge coordination number is higher than the solid contact coordination number (Fig. 13b). This is because that a water bridge may exist between two neighbouring particles without a physical contact. With axial deformation, the water bridge coordination numbers for the loose and dense specimens also evolve to the same value, corresponding to the critical state degree of saturation.

Similarly, the directional mean contact and capillary force evolutions in the same set of triaxial tests are demonstrated in Fig. 14. In the wet material, the mean contact force is larger than that of the dry material due to the water bridge effect (Fig. 14a). The maximum contact force in the dense material is higher than that of the loose specimen. By shearing to 40% axial strain, the ultimate mean contact forces are stable and have unique values for dry and wet materials respectively. Fig. 14b also indicates that at critical state the mean capillary forces become the same for both dense and loose samples.

In Eq. 16, the scalars determining the mean stress level, and the direction tensors, which quantify the solid contact fabric, solid contact force network and water bridge fabric respectively, ascertain the magnitude of stress deviator. The evolutions of the anisotropy of these tensors are then presented in Fig. 15. In Fig. 15a, the solid contact fabric becomes anisotropic upon loading from the initial isotropic state.

The maximum solid fabric anisotropy is higher in the dense material, but the ultimate fabric anisotropy is the same for materials with different initial void ratios. For the wet materials with a constant suction, the induced solid phase fabric anisotropy $(D_1^s - D_3^s)$ is lower than that of the dry material. There is also a unique fabric anisotropy at the critical state. In Fig. 15b, regarding the solid contact force anisotropy $(G_1^{sf} - G_3^{sf})$, the initial void ratio influences its maximum value but the ultimate value is also the same. It also indicates that the capillary effect has little influence on the contact force anisotropy evolution. However, this doesn't mean that the cohesive capillary force has no influence on the force transmission pattern. As [44] already introduced that the capillary bridges increased the possibility of weak interparticle contact forces. These forces didn't change the contact force anisotropy index, which is based on a tensorial form calculation. In Fig. 15c, the anisotropy of the joint tensor term is obviously altered by capillary bridge. Although the water bridge distribution is not the same as the solid contact distribution, it is indeed affected by the solid structure and become anisotropic upon triaxial loading (Fig. 15d). The water phase anisotropy $(D_1^w - D_3^w)$ evolution in Fig. 15d also shows that there may also be a critical state value for each suction.

4.2 Critical state stress ratio and fabric anisotropies

After the stress-force-fabric relationship in Eq. 16, the mean stress, sum of the mean contact stress and the mean capillary stress, can be formulated by the scalar micro parameters as:

$$\mathrm{p} = \mathrm{p}_{\mathrm{cont}} + \mathrm{p}_{\mathrm{cap}} \approx \frac{\mathrm{N}\overline{\mathrm{R}}}{3\mathrm{V}} \omega_{\mathrm{s}} \, \mathrm{f}_{\mathrm{cont0}} + \frac{\mathrm{N}\overline{\mathrm{R}}}{3\mathrm{V}} \omega_{\mathrm{w}} \, \mathrm{f}_{\mathrm{cap0}} \tag{17}$$

After Eq. 16, the deviatoric stress, which is associated with the anisotropy effects in the direction tensors, can be approximately written as:

$$\mathrm{q} \approx \frac{\mathrm{N}\overline{\mathrm{R}}}{3\mathrm{V}} \omega_{\mathrm{s}} \, \mathrm{f}_{\mathrm{cont0}} \left[(\mathrm{G}_1^{\mathrm{sf}} - \mathrm{G}_3^{\mathrm{sf}}) + \frac{2}{5}(\mathrm{D}_1^{\mathrm{s}} - \mathrm{D}_3^{\mathrm{s}}) + \frac{2}{5}(\mathrm{D}_1^{\mathrm{s}}\mathrm{G}_1^{\mathrm{sf}} - \mathrm{D}_3^{\mathrm{s}}\mathrm{G}_3^{\mathrm{sf}}) \right] + \frac{\mathrm{N}\overline{\mathrm{R}}}{3\mathrm{V}} \omega_{\mathrm{w}} \, \mathrm{f}_{\mathrm{cap0}} \frac{2}{5}(\mathrm{D}_1^{\mathrm{w}} - \mathrm{D}_3^{\mathrm{w}}) \tag{18}$$

We can denote $\Delta G^{sf} = \left(G_1^{sf} - G_3^{sf}\right)$ as the anisotropy in contact forces, $\Delta D^s = (D_1^s - D_3^s)$ as the solid contact fabric anisotropy, $\Delta D^s G^{sf} = \left(D_1^s G_1^{sf} - D_3^s G_3^{sf}\right)$ as the joint tensor anisotropy and $\Delta D^w = (D_1^w - D_3^w)$ as the water phase fabric anisotropy. Thus, the stress ratio can be formulated as:

$$\frac{\mathrm{q}}{\mathrm{p}} \approx \frac{\omega_{\mathrm{s}} \, \mathrm{f}_{\mathrm{cont0}}}{\omega_{\mathrm{s}} \, \mathrm{f}_{\mathrm{cont0}} + \omega_{\mathrm{w}} \, \mathrm{f}_{\mathrm{cap0}}} \left(\Delta \mathrm{G}^{\mathrm{sf}} + \frac{2}{5}\Delta \mathrm{D}^{\mathrm{s}} + \frac{2}{5}\Delta \mathrm{D}^{\mathrm{s}}\mathrm{G}^{\mathrm{sf}} \right) + \frac{\omega_{\mathrm{w}} \, \mathrm{f}_{\mathrm{cap0}}}{\omega_{\mathrm{s}} \, \mathrm{f}_{\mathrm{cont0}} + \omega_{\mathrm{w}} \, \mathrm{f}_{\mathrm{cap0}}} \frac{2}{5} \Delta \mathrm{D}^{\mathrm{w}} \tag{19}$$

As $\frac{p_{cont}}{p} = \frac{\omega_s f_{cont_0}}{\omega_s f_{cont_0} + \omega_w f_{cap_0}}$ and $\frac{p_{cap}}{p} = \frac{\omega_w f_{cap_0}}{\omega_s f_{cont_0} + \omega_w f_{cap_0}}$ (from Eq. 16), combining Eq. 19 with Eq. 13, the critical state parameters for stress ratio can then be linked to the internal fabric and force anisotropies as:

$$M_s \approx \Delta G^{sf} + \frac{2}{5}\Delta D^s + \frac{2}{5}\Delta D^s G^{sf} \tag{20}$$

and:

$$M_w \approx \frac{2}{5}\Delta D^w \tag{21}$$

Fig. 16 demonstrates the critical state fabric and force anisotropies in different mean stress levels. The solid contact anisotropy is depicted in Fig. 16a. For a dry material, the critical state solid fabric anisotropy is reduced by the mean stress increase. In a low stress state, when the capillary effect is applied, the magnitude of critical state solid fabric anisotropy is reduced significantly from its dry state value. With the increase of mean stress, solid fabric anisotropy at critical state has a raise-and-fall trend. The discrepancies of solid fabric anisotropy between the dry and wet materials are also reduced by mean stress. Fig. 16b shows the solid contact force anisotropy quantified by tensor G_{ij}^{sf}. It indicates that the capillary bridge effect on contact force anisotropy is not significant. With the logarithmic increase of mean stress, the contact force anisotropy at critical state raises almost linearly. The anisotropy of the joint tensor $D_{im}^{s}G_{jm}^{sf}$, depicted in Fig. 16c, is generally a negative value. For the dry material, the anisotropy of the joint tensor is almost constant for different mean stresses. However, in the wet materials, the joint tensor anisotropy is higher in the low stress conditions and is reduced with mean stress increase. The critical state anisotropy of the water phase, represented by the water bridge direction anisotropy in Fig. 16d, is rather constant under different mean stress conditions. It also shows that with a higher suction, which means a lower degree of saturation, the critical state water phase anisotropy is more significant.

The anisotropy values of different components can be summed up according to Eq. 20 to estimate M_s. In the previous section, M_s was taken as a constant value 0.73 for all stress conditions for model simplicity. In Fig. 17a, it shows that the M_s values estimated from the internal force and fabric anisotropies are not always constant. There is an overestimation at low stress levels by taking $M_s = 0.73$, especially for the wet materials. Fig. 17b presents the M_w values estimated from the critical state water fabric anisotropy as a function of the degree of saturation. As the water phase fabric anisotropy is not influenced by mean stress obviously. The average value was taken for each applied suction and the relationship between $\frac{2}{5}\Delta D^w$ and degree of saturation is then obtained. It shows that $\frac{2}{5}\Delta D^w$ (the triangles) has a similar trend with the measured M_w values in Table 2 but is however lower than the measured value (the dashed line). This is due to the fact that the constant approximation of $M_s = 0.73$ was taken for simplicity. Therefore, the deviatoric effect of the contact stress in low stress conditions was overestimated and was actually corrected by the M_w values in Table 2. The correction in M_w values is about 0.21 by evaluating the difference between the M_w values and the $\frac{2}{5}\Delta D^w$ values. It can be seen that when $\frac{2}{5}\Delta D^w$ is shifted up by 0.21 they coincide with the measured M_w values. By following that M_w is associated with the water phase anisotropy effect, one may deduce that the second trend in Fig. 11b, as M_w converges to 0 at saturation, is more realistic. This is because, as it can be easily understood, at full saturation the water phase effect becomes isotropic.

4.3 The relationship between scalar micro-parameters and mean stress level

From the macro observations, it has already been know that capillary effect is less prominent under high stress conditions. A more insightful understanding can also be achieved by analysing its micro-structures and force transmissions. From Eq. 17, it can be seen that the mean contact stress and the mean capillary stress are related to the coordination numbers (ω_s and ω_w) and mean forces (${f_{cont}}_0$ and ${f_{cap}}_0$). Fig. 18a demonstrates the critical state mean contact stress under different mean total stress levels. For dry materials, $p_{cont} = p$ and for wet granular materials p_{cont} is higher. It shows that the capillary effect is more significant when $p < 100kPa$. From Eq. 17, p_{cont} is microscopically determined by the solid contact coordination number and mean contact force. Fig. 18b depicts the critical state solid contact coordination numbers under various mean stress and suctions. For a dry material, the solid contact coordination number at critical state is positively related to its mean stress. The dilatancy of wet granular materials is generally higher in triaxial shear, which leads a higher critical state void ratio. Therefore, the critical state solid contact coordination numbers of wet materials are generally higher than that of the dry material. With the increase of mean stress, the critical state ω_s values for wet granular materials are gradually reduced and they increase again to approach to the ω_s values for the dry material at high stress conditions. In Fig. 18c, the mean contact force is increased linearly with mean stress level and when the mean stress is relatively low, the capillary effect has more significant influence on ${f_{cont}}_0$, which leads ${f_{cont}}_0$ to be higher than that of the dry material.

Fig. 19a presents the critical state mean capillary stress at different suctions and mean stress levels. The capillary stress is a negative stress and with the increase of suction, which means a decrease in water content, the absolute value of mean capillary stress is lower. It also indicates that the mean capillary stress is not changed obviously by the mean total stress increase. As the mean capillary stress is related to the water bridge coordination number and mean capillary force (from Eq. 17), the ω_w and ${f_{cap}}_0$ values at critical state are presented in Fig. 19b and Fig. 19c respectively. It can be observed that ω_w and ${f_{cap}}_0$ values are not obviously altered by the mean total stress. The ${f_{cap}}_0$ value is negative as capillary force is an attractive force. With the increase of suction (a decrease of water content), the water bridge coordination number is reduced and the magnitude of the capillary force (its absolute value) is larger.

5. Conclusions

In this paper, the critical state of wet granular materials is systematically investigated by series of DEM simulations. Water bridge effect is considered between neighbouring particles providing the material has a relatively low degree of saturation in the residual state (the pendular state). By testing relatively dense and loose materials in different suctions in the conventional triaxial loading path, the critical state is reached in both macro stress-strain behaviours and micro structures. Main conclusions can be drawn from both macro and micro aspects as follows:

1. The contact stress tensor, which is formulated by inter-particle mechanical forces, is not sufficient to be used as the effective stress of unsaturated granular materials to model the critical state behaviours. It can model the critical state with a linear mean contact stress and deviatoric contact stress relationship (in the p-q space). However, due to the higher dilatancy in wet materials, solely using contact stress is not enough to describe the deformation and critical state void ratio (in the p-e space).
2. The critical state stress ratio for wet materials is not constant as it is much higher under a low mean total stress. Critical state equations (Eq. 12 to Eq. 15) are proposed to fit the simulated critical state stress ratio and void ratio by using the mean contact stress (p_{cont}) and mean capillary stress (p_{cap} or $p - p_{cont}$). Classic parameters for dry or fully saturated conditions are kept with one more term added to quantify the capillary stress effect in each equation. The parameter associated with capillary stress is correlated to suction or degree of saturation.
3. As reported before [48], the stress state is related to the internal structure indexed by the micro quantities such as the solid contact coordination number, water bridge number, solid and water phase fabric tensors and contact force and capillary force levels and anisotropies. It has been observed in this study that at the critical state, unique values have been reached in these micro quantities.
4. By analysing the deviatoric stress and mean stress with the stress-force-fabric relationship equation, it is realised that the two parameters for the critical state stress ratio in the proposed critical state equations (M_s and M_w) are related to the critical state internal solid structure anisotropy and the water phase fabric anisotropy respectively. This also implies that at full saturation, the parameter M_w is possibly converged to 0, as the water phase is an isotropic effect at full saturation.
5. At the critical state, the mean capillary stress is almost independent of the mean total stress. This is because the water bridge coordination number and the mean capillary force are almost not affected by the total stress level. The solid contact coordination number and mean contact force are obviously increased by the capillary effect especially in low stress conditions which induce a more significant mean contact stress when in low stress conditions.

Appendix: Calculation of direction tensors

For a granular assembly with N_s solid contacts (note that one physical contact point has two contacts), after Oda et al. [23], a moment tensor quantifying the directions of solid contact normals can be expressed as:

$$\mathrm{N}_{ij}^{s} = \frac{1}{\mathrm{N}_s} \sum_{c \in V} \mathbf{n}_c \otimes \mathbf{n}_c \tag{22}$$

where $\boldsymbol{n_c}$ is the unit vector of the contact normal on the c-th solid contact. Similarly, a second rank tensor for water bridge network can also be raised. For a sample with N_w particle water interactions (two times of total water bridge number), the moment tensor can be written as:

$$\mathrm{N}_{ij}^{w} = \frac{1}{\mathrm{N}_w} \sum_{w \in V} \mathbf{n}_w \otimes \mathbf{n}_w \tag{23}$$

where $\boldsymbol{n_w}$ is the unit vector pointing from water bridge centre to particle centre on the w-th water-solid interaction. The direction tensors of D_{ij}^{s} and D_{ij}^{w} consider the deviatoric part of the moment tensor being formulated as:

$$\mathrm{D}_{ij}^{s/w} = \frac{15}{2}\left(\mathrm{N}_{ij}^{s/w} - \frac{1}{3}\delta_{ij} \right) \tag{24}$$

by taking the corresponding superscript.

For the directional distribution of contact forces, a second rank moment tensor is also defined. By integrating the tensor product of the average contact force along a particular direction, the moment tensor noted as K_{ij}^{sf}, can be expressed in a unit sphere space Ω as:

$$\mathrm{K}_{ij}^{sf} = \frac{1}{2\pi} \frac{1}{\mathrm{N}_s} \oint_{\Omega} \left\langle \mathbf{f}_{\mathbf{cont}} \right\rangle\Big|_{\mathbf{n}_c} \otimes \mathbf{n}_c \mathrm{d}\Omega \tag{25}$$

where $\langle \mathbf{f}_{\mathbf{cont}} \rangle|_{\mathbf{n_c}}$ is the average value for the contact forces in the $\boldsymbol{n_c}$ direction. The direction tensor of contact force, G_{ij}^{sf}, is the deviatoric part of the contact force moment tensor in a normalised form:

$$\mathrm{G}_{ij}^{sf} = \frac{3\mathrm{K}_{ij}^{sf}}{\mathrm{K}_{11}^{sf} + \mathrm{K}_{22}^{sf} + \mathrm{K}_{33}^{sf}} - \delta_{ij} \tag{26}$$

Note that the directional mean contact force is ${f_{cont}}_0 \approx K_{11}^{sf} + K_{22}^{sf} + K_{33}^{sf}$. Similar to the above procedures, the directional mean capillary force ${f_{cap}}_0$ can also be obtained from a moment tensor for the capillary forces which will not be repeated.

Acknowledgement

The authors would like to thank the high performance computing service at the University of Nottingham for implementing the DEM simulation programmes. The first author also appreciates the support of Taishan Scholar Project of Shandong Province of China during paper writing and revision.

Conflict of Interest

The author states that there is no conflict of interest.

References

1. Alonso EE, Gens A, Josa A (1990) A constitutive model for partially saturated soils. Géotechnique 40:405–430. doi: 10.1680/geot.1990.40.3.405

2. Been K, Jefferies M, Hachey J (1991) The critical state of sands. Geotechnique 41:365–381

3. Been K, Jefferies MG (1985) A state parameter for sands. Géotechnique 35:99–112. doi: 10.1016/0148-9062(85)90263-3

4. Berger N, Azéma E, Douce J-F, Radjai F (2015) Scaling behaviour of cohesive granular flows. EPL (Europhysics Lett 112:64004. doi: 10.1209/0295-5075/112/64004

5. Bishop AW, Blight GE (1963) Some Aspects of Effective Stress in Saturated and Partly Saturated Soils. Géotechnique 13:177–197. doi: 10.1680/geot.1963.13.3.177

6. Chalak C, Chareyre B, Nikooee E, Darve F (2017) Partially saturated media: from DEM simulation to thermodynamic interpretation. Eur J Environ Civ Eng 21:798–820. doi: 10.1080/19648189.2016.1164087

7. Christoffersen J, Mehrabadi MM, Nemat-Nasser S (1981) A Micromechanical Description of Granular Material Behavior. J Appl Mech 48:339. doi: 10.1115/1.3157619

8. Cundall PA, Strack ODL (1979) A discrete numerical model for granular assemblies. Géotechnique 29:47–65. doi: 10.1680/geot.1979.29.1.47

9. Delenne J-Y, Richefeu V, Radjai F (2015) Liquid clustering and capillary pressure in granular media. J Fluid Mech 762:R5. doi: 10.1017/jfm.2014.676

10. Duriez J, Wan R (2017) Contact angle mechanical influence in wet granular soils. Acta Geotech 12:67–83. doi: 10.1007/s11440-016-0500-6

11. Duriez J, Wan R, Pouragha M, Darve F (2018) Revisiting the existence of an effective stress for wet granular soils with micromechanics. Int J Numer Anal Methods Geomech 42:959–978. doi: 10.1002/nag.2774

12. Gabrieli F, Lambert P, Cola S, Calvetti F (2012) Micromechanical modelling of erosion due to evaporation in a partially wet granular slope. Int J Numer Anal Methods Geomech 36:918–943. doi: 10.1002/nag.1038

13. Gallipoli D, Gens A, Chen G, D'Onza F (2008) Modelling unsaturated soil behaviour during normal consolidation and at critical state. Comput Geotech 35:825–834. doi: 10.1016/j.compgeo.2008.08.006

14. Huang X, Hanley KJ, O'Sullivan C, Kwok CY, Wadee MA (2014) DEM analysis of the influence of the intermediate stress ratio on the critical-state behaviour of granular materials. Granul Matter 16:641–655. doi: 10.1007/s10035-014-0520-6

15. Jefferies M, Been K (2000) Implications for critical state theory from isotropic compression of sand. Géotechnique 50:419–429. doi: 10.1680/geot.2000.50.4.419

16. Khamseh S, Roux J-N, Chevoir F (2015) Flow of wet granular materials: A numerical study. Phys Rev E 92:022201. doi: 10.1103/PhysRevE.92.022201

17. Kloss C, Goniva C, Hager A (2012) Models, algorithms and validation for opensource DEM and CFD–DEM. Prog Comput Fluid Dyn an Int J 12:140–152

18. Kuhn MR (2016) The critical state of granular media: convergence, stationarity and disorder. Géotechnique 66:902–909. doi: 10.1680/jgeot.16.P.008

19. Li X-S, Dafalias Y (2012) Anisotropic critical state theory: role of fabric. J Eng Mech 138:263–275. doi: 10.1061/(ASCE)EM.1943-7889.0000324.

20. Li X-S, Dafalias YF, Wang Z-L (1999) State-dependant dilatancy in critical-state constitutive modelling of sand. Can Geotech J 36:599–611. doi: 10.1139/t99-029

21. Li X, Yu H-S (2013) On the stress--force--fabric relationship for granular materials. Int J Solids Struct 50:1285–1302. doi: 10.1016/j.ijsolstr.2012.12.023

22. Lu N, Godt JW, Wu DT (2010) A closed-form equation for effective stress in unsaturated soil. Water Resour Res 46:W05515. doi: 10.1029/2009WR008646

23. Oda M, Konishi J, Nemat-Nasser S (1982) Experimental micromechanical evaluation of strength of granular materials: Effects of particle rolling. Mech Mater 1:269–283. doi: 10.1016/0167-6636(82)90027-8

24. Radjai F, Richefeu V (2009) Bond anisotropy and cohesion of wet granular materials. Philos Trans A Math Phys Eng Sci 367:5123–5138. doi: 10.1098/rsta.2009.0185

25. Richefeu V, Radjai F, Delenne J-Y (2016) Lattice Boltzmann modelling of liquid distribution in unsaturated granular media. Comput Geotech 80:353–359. doi: 10.1016/j.compgeo.2016.02.017

26. Richefeu V, El Youssoufi M, Radjaï F (2006) Shear strength properties of wet granular materials. Phys Rev E 73:051304. doi: 10.1103/PhysRevE.73.051304

27. Roscoe KH, Schofield AN, Wroth CP (1958) On The Yielding of Soils. Géotechnique 8:22–53. doi: 10.1680/geot.1958.8.1.22

28. Rothenburg L, Bathurst RJ (1989) Analytical study of induced anisotropy in idealized granular materials. Géotechnique 39:601–614. doi: 10.1680/geot.1989.39.4.601

29. Roy S, Luding S, Weinhart T (2017) A general(ized) local rheology for wet granular materials. New J Phys 19:043014. doi: 10.1088/1367-2630/aa6141

30. Scheel M, Seemann R, Brinkmann M, Di Michiel M, Sheppard A, Breidenbach B, Herminghaus S (2008) Morphological clues to wet granular pile stability. Nat Mater 7:189–193. doi: 10.1038/nmat2117

31. Schofield A, Wroth P (1968) Critical state soil mechanics. McGraw-Hill, London

32. Scholtès L, Chareyre B, Nicot F, Darve F (2009) Micromechanics of granular materials with capillary effects. Int J Eng Sci 47:64–75. doi: 10.1016/j.ijengsci.2008.07.002

33. Scholtès L, Hicher P, Nicot F, Chareyre B, Darve F (2009) On the capillary stress tensor in wet granular materials. Int J Numer Anal Methods Geomech 33:1289–1313. doi: 10.1002/nag.767

34. El Shamy U, Gröger T (2008) Micromechanical aspects of the shear strength of wet granular soils. Int J Numer Anal Methods Geomech 32:1763–1790. doi: 10.1002/nag.695

35. Shen Z, Jiang M, Thornton C (2016) Shear strength of unsaturated granular soils: three-dimensional discrete element analyses. Granul Matter 18:37. doi: 10.1007/s10035-016-0645-x

36. Singh A, Magnanimo V, Saitoh K, Luding S (2015) The role of gravity or pressure and contact stiffness in granular rheology. New J Phys 17:043028. doi: 10.1088/1367-2630/17/4/043028

37. Sitharam TG, Vinod JS (2008) Critical state behaviour of granular materials from isotropic and rebounded paths: DEM simulations. Granul Matter 11:33–42. doi: 10.1007/s10035-008-0113-3

38. Soulié F, Cherblanc F, El Youssoufi MS, Saix C (2006) Influence of liquid bridges on the mechanical behaviour of polydisperse granular materials. Int J Numer Anal Methods Geomech 30:213–228. doi: 10.1002/nag.476

39. Tarantino A (2007) A possible critical state framework for unsaturated compacted soils. Géotechnique 57:385–389. doi: 10.1680/geot.2007.57.4.385

40. Toll DG (1990) A framework for unsaturated soil behaviour. Géotechnique 40:31–44. doi: 10.1680/geot.1990.40.1.31

41. Toll DG, Ali Rahman Z (2017) Critical state shear strength of an unsaturated artificially cemented sand. Géotechnique 67:208–215. doi: 10.1680/jgeot.15.P.042

42. Toll DG, Ong BH (2003) Critical-state parameters for an unsaturated residual sandy clay. Géotechnique 53:93–103. doi: 10.1680/geot.2003.53.1.93

43. Wan R, Duriez J, Darve F (2015) A tensorial description of stresses in triphasic granular materials with interfaces. Geomech Energy Environ 4:73–87. doi: 10.1016/j.gete.2015.11.004

44. Wang J-P (2017) Force Transmission Modes of Non-Cohesive and Cohesive Materials at the Critical State. Materials (Basel) 10:1014. doi: 10.3390/MA10091014

45. Wang J-P, François B, Lambert P (2017) Equations for hydraulic conductivity estimation from particle size distribution: A dimensional analysis. Water Resour Res 53:8127–8134. doi: 10.1002/2017WR020888

46. Wang J-P, Gallo E, François B, Gabrieli F, Lambert P (2017) Capillary force and rupture of funicular liquid bridges between three spherical bodies. Powder Technol 305:89–98. doi: 10.1016/j.powtec.2016.09.060

47. Wang J-P, Hu N, François B, Lambert P (2017) Estimating water retention curves and strength properties of unsaturated sandy soils from basic soil gradation parameters. Water Resour Res 53:6069–6088. doi: 10.1002/2017WR020411

48. Wang J-P, Li X, Yu H-S (2017) Stress–Force–Fabric Relationship for Unsaturated Granular Materials in Pendular States. J Eng Mech 143:04017068. doi: 10.1061/(ASCE)EM.1943-7889.0001283

49. Wang J-P, Li X, Yu H-S (2018) A micro–macro investigation of the capillary strengthening effect in wet granular materials. Acta Geotech 13:513–533. doi: 10.1007/s11440-017-0619-0

50. Wang K, Sun W (2017) Anisotropy of a Tensorial Bishop's Coefficient for Wetted Granular Materials. J Eng Mech 143:B4015004. doi: 10.1061/(ASCE)EM.1943-7889.0001005

51. Wang Q, Pufahl DE, Fredlund DG (2002) A study of critical state on an unsaturated silty soil. Can Geotech J 39:213–218. doi: 10.1139/t01-086

52. Wheeler SJ, Sivakumar V (1995) An elasto-plastic critical state framework for unsaturated soil. Géotechnique 45:35–53. doi: 10.1680/geot.1995.45.1.35

53. Zhao J, Guo N (2013) Unique critical state characteristics in granular media considering fabric anisotropy. Géotechnique 63:695–704. doi: 10.1680/geot.12.P.040

54. Zhou W, Liu J, Ma G, Chang X (2017) Three-dimensional DEM investigation of critical state and dilatancy behaviors of granular materials. Acta Geotech 12:527–540. doi: 10.1007/s11440-017-0530-8

Figure List

Fig. 1. Contact model with capillary bridge effect.

Fig. 2. Isotropic normal consolidation lines.

Fig. 3. Water retention curves under different confinements.

Fig. 4. Conventional triaxial loading path.

Fig. 5. Typical triaxial test results of dry and wet granular materials ($S = 20kPa$) to the critical state ($\sigma_2 = \sigma_3 = 10kPa$). (a) Evolution of deviatoric stress; (b) Evolution of volumetric strain; (c) Evolution of void ratio; (d) Evolution of degree of saturation.

Fig. 6. Critical state deviatoric stress at different mean stress levels. (a) $p - q$ line; (b) $p' - q$ line; (c) $p_{cont} - q$ line; (d) $p_{cont} - q_{cont}$ line.

Fig. 7. Critical state void ratio in $p_{cont} - e$ space.

Fig. 8. Critical state stress ratio and deviatoric stress in the framework. (a) $p - M$ relationship; (b) $p - q$ relationship.

Fig. 9. Correlation between bond number and critical state stress ratio.

Fig. 10. Critical state void ratio in the framework.

Fig. 11. The degree of saturation effect on critical state stress ratio parameters. (a) The results from DEM simulations; (b) Hypothetical trend beyond the pendular state.

Fig. 12. The degree of saturation effect on λ_w.

Fig. 13. Evolution of coordination numbers in triaxial shearing. (a) Coordination number of solid contacts; (b) Coordination number of water-solid interactions.

Fig. 14. Evolutions of mean contact and capillary forces in triaxial shearing. (a) Mean contact force; (b) Mean capillary force.

Fig. 15. Evolutions of internal fabric and force anisotropies. (a) Solid contact fabric anisotropy; (b) solid contact force anisotropy; (c) Water bridge network anisotropy.

Fig. 16. The critical state fabric and force anisotropies at different mean stress levels. (a) Solid fabric anisotropy; (b) Solid contact force anisotropy; (c) The joint tensor anisotropy; (d) Water fabric anisotropy.

Fig.17. The critical state stress ratio parameters and internal fabric anisotropy. (a) Comparison with parameter M_s; (b) Comparison with parameter M_w.

Fig. 18. The critical state mean contact stress and its associated micro-parameters at different mean total stress levels. (a) Mean contact stress; (b) Solid contact coordination number; (c) Directional mean contact force.

Fig. 19. The critical state mean capillary stress and its associated micro-parameters at different mean total stress levels. (a) Mean capillary stress; (b) Water bridge coordination number; (c) Directional mean capillary force.

Table List

Table 1. Summary of triaxial test parameters.

Table 2. Summary of critical state parameters.

Table 1

$\sigma_2\&\sigma_3$ / S (kPa)	10kPa	20kPa	50kPa	100kPa	200kPa	500kPa	1MPa	2MPa	5MPa	10MPa	20MPa	50MPa
dry	√	√	√	√	√	√	√	√	√	√	√	√
5000	√	√	√	√	√	√	√	√	–	√	–	–
700	√	√	√	√	√	√	√	√	–	–	–	–
300	√	√	√	√	√	√	√	√	–	–	–	–
200	√	√	√	√	√	√	√	√	–	–	–	–
100	√	√	√	√	√	√	√	√	–	–	–	–
50	√	√	√	√	√	√	√	√	–	–	–	–
20	√	√	√	√	√	√	√	√	–	√	–	–

*Both the dense and loose specimens are tested on each set of parameter. √ means triaxial tests have been implemented.

Table 1. Summary of triaxial test parameters.

Table 2

Suction (kPa)	S_r **(%)**	M_s	M_w	Γ_s	λ_s	λ_w
dry	0	0.73	0.73	1.755	9.89×10^{-5}	0
5000	0.000876		0.59			0.0407
700	0.042		0.42			0.0398
300	0.196		0.38			0.0427
200	0.411		0.37			0.0432
100	1.19		0.33			0.0484
50	3.39		0.24			0.0337
20	9.75		0.22			0.0404

Table 2. Summary of critical state parameters.

Figures

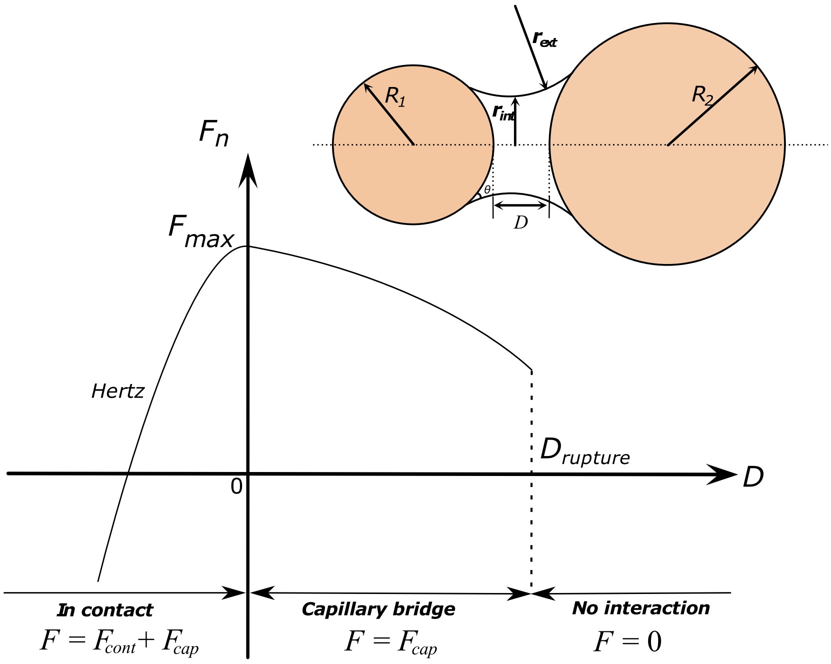

Figure 1: Contact model with capillary bridge effect

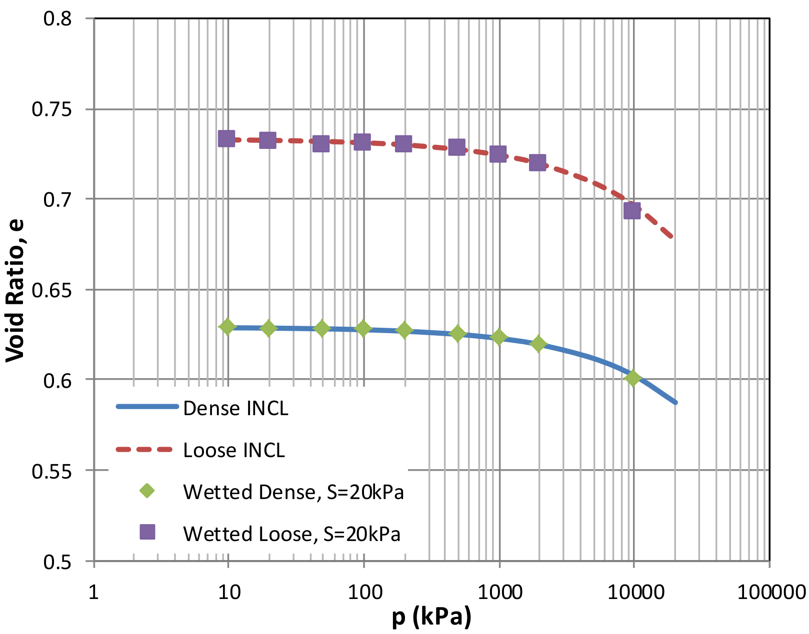

Figure 2: Isotropic normal consolidation lines

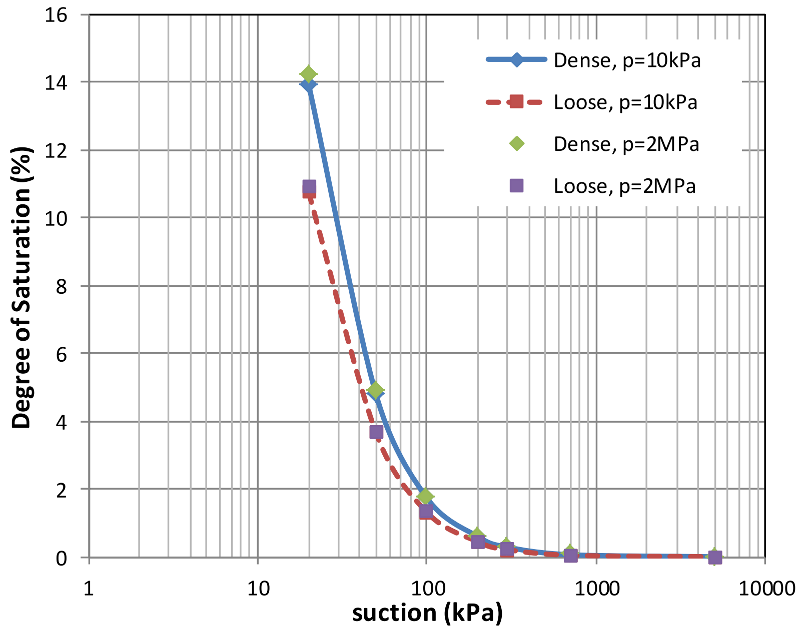

Figure 3: Water retention curves under different confinements

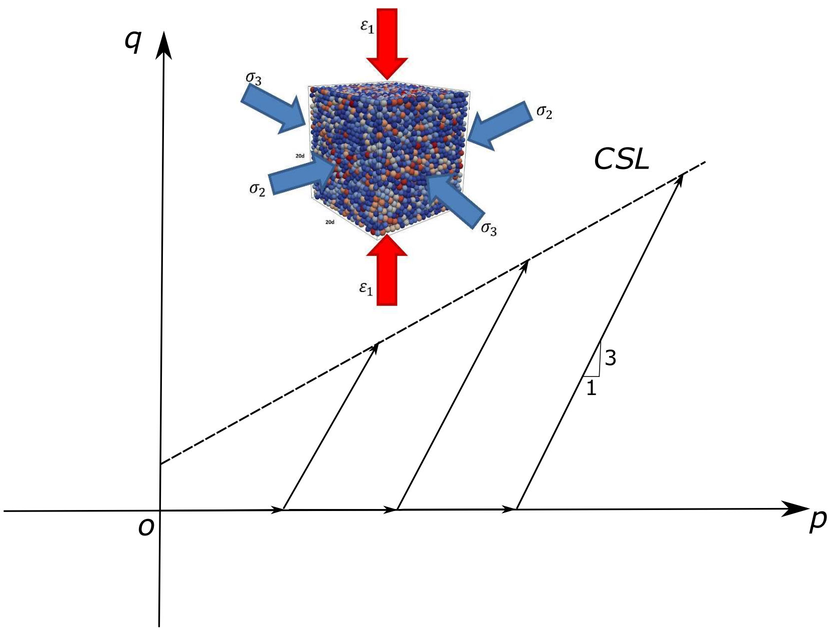

Figure 4: Conventional triaxial loading path

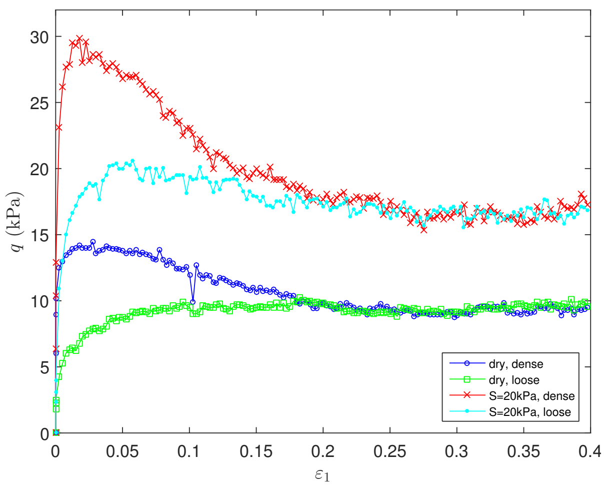

(a) Evolution of deviatoric stress

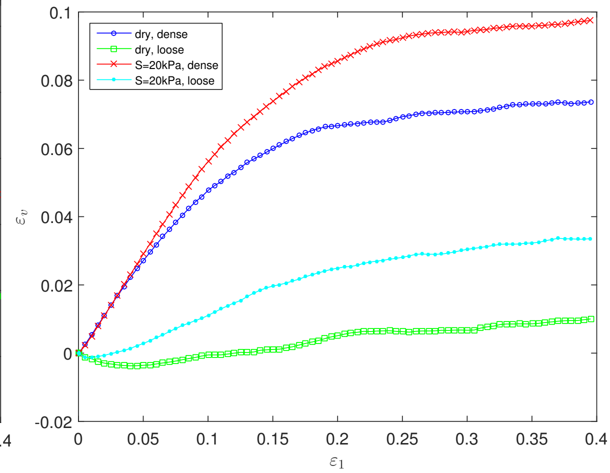

(b) Evolution of volumetric strain

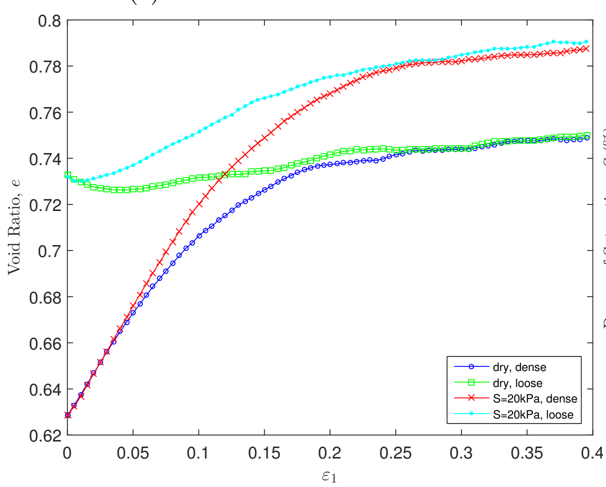

(c) Evolution of void ratio

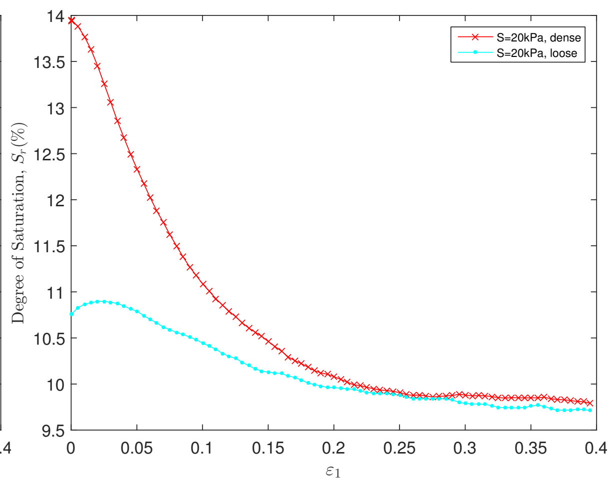

(d) Evolution of degree of saturation

Figure 5: Typical triaxial test results of dry and wet granular materials ($S = 20kPa$) to the critical state ($\sigma_2 = \sigma_3 = 10kPa$).

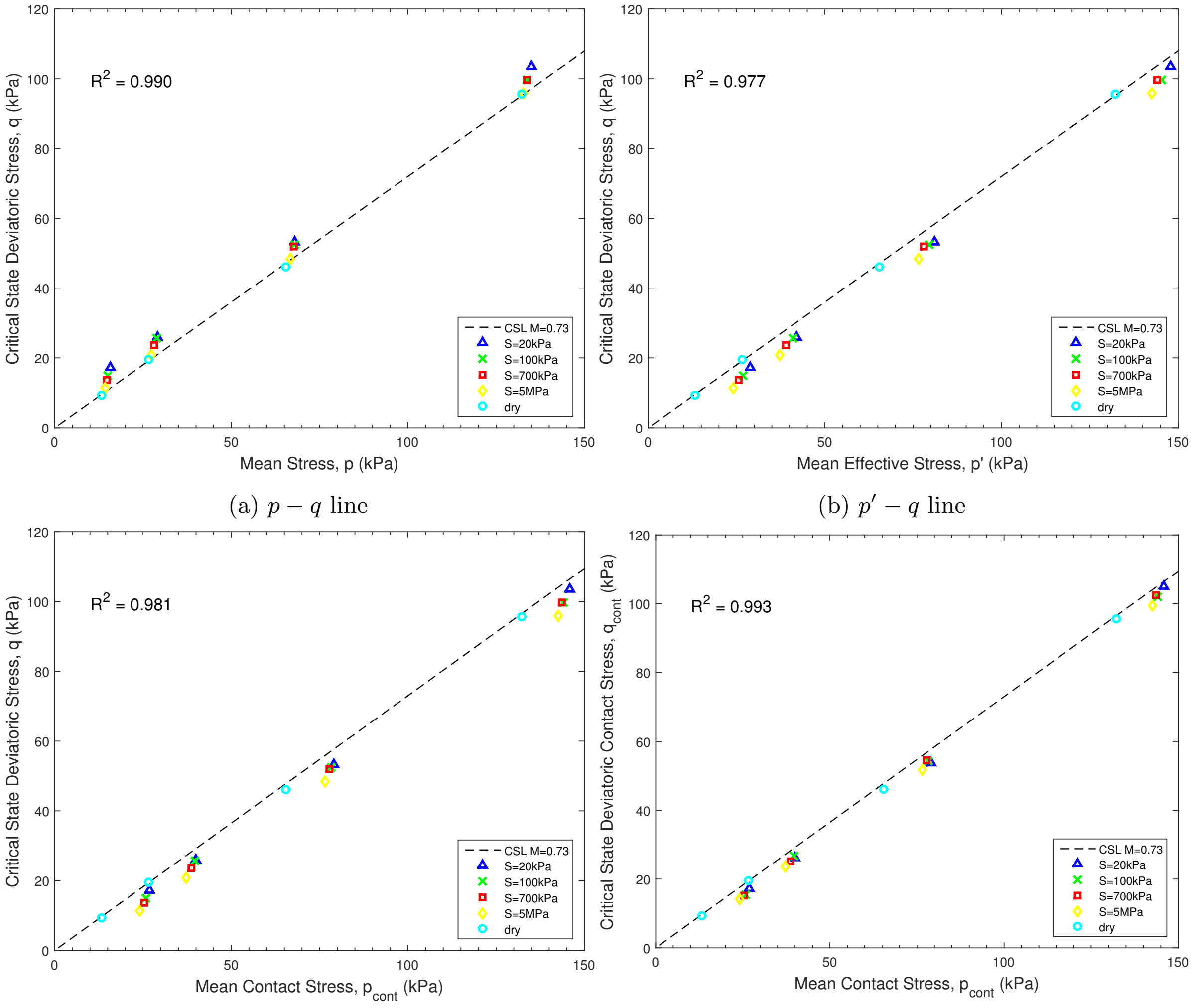

(a) $p - q$ line

(b) $p' - q$ line

(c) $p_{cont} - q$ line

(d) $p_{cont} - q_{cont}$ line

Figure 6: Critical state deviatoric stress at different mean stress levels.

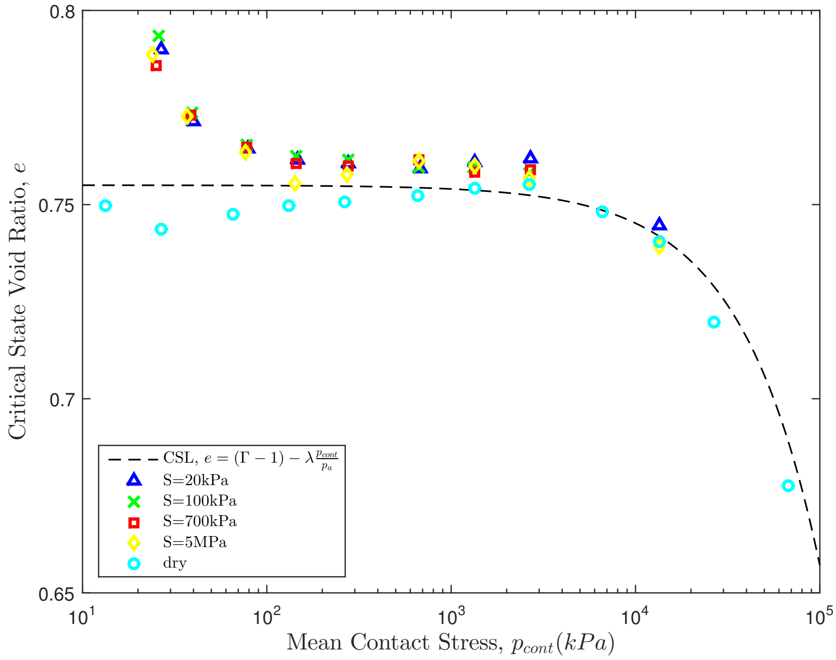

Figure 7: Critical state void ratio in $p_{cont} - e$ space.

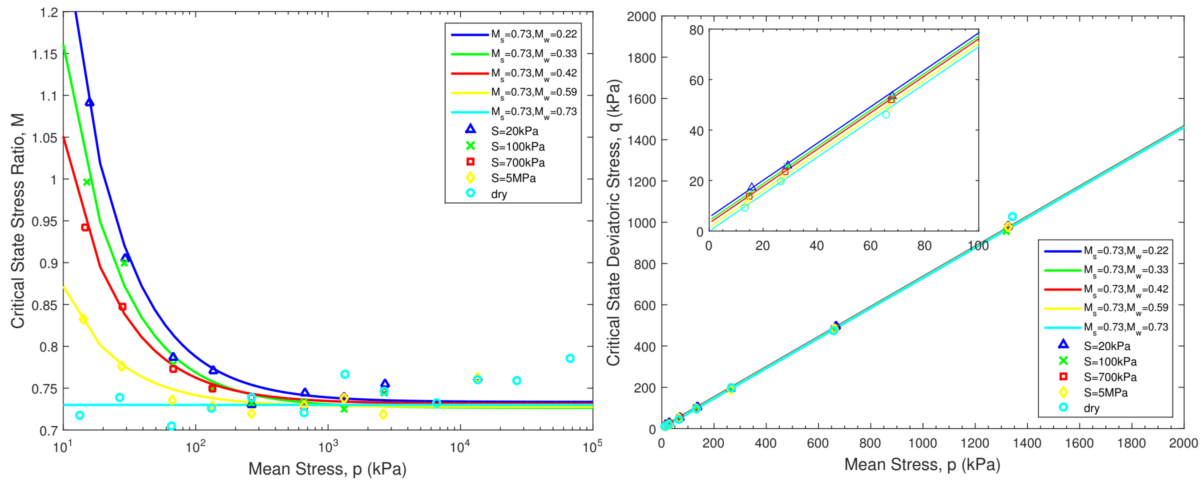

(a) $p - M$ relationship

(b) $p - q$ relationship

Figure 8: Critical state stress ratio and deviatoric stress in the framework.

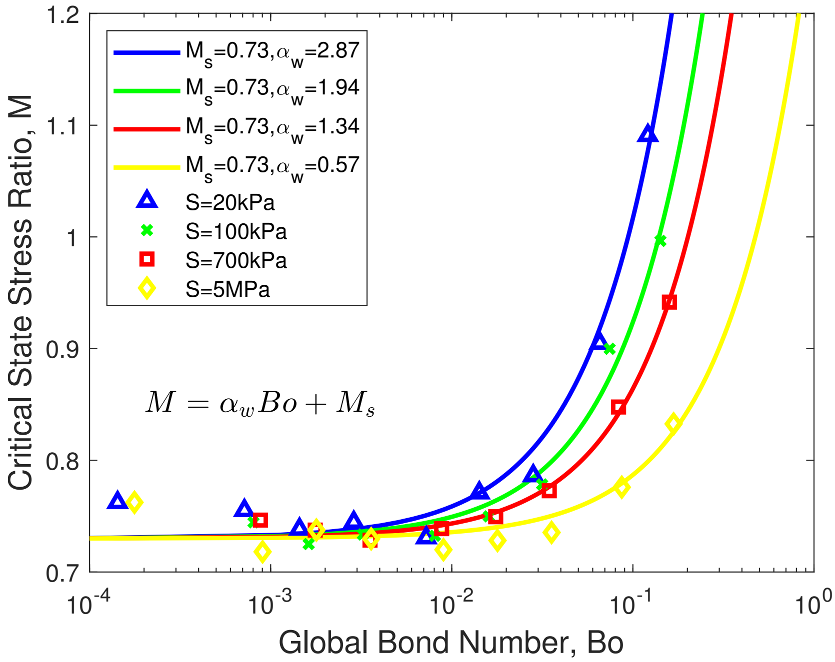

Figure 9: Correlation between bond number and critical state stress ratio.

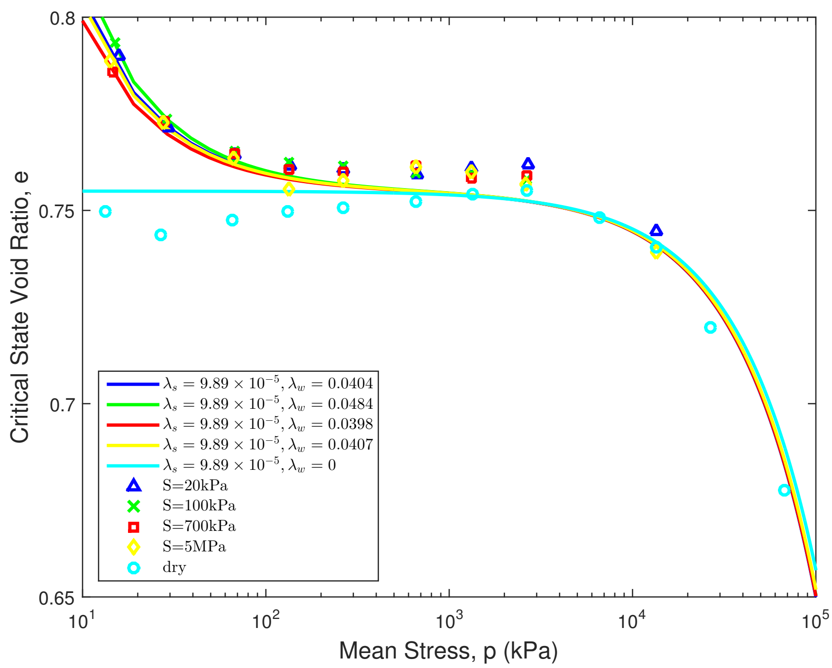

Figure 10: Critical state void ratio in the framework.

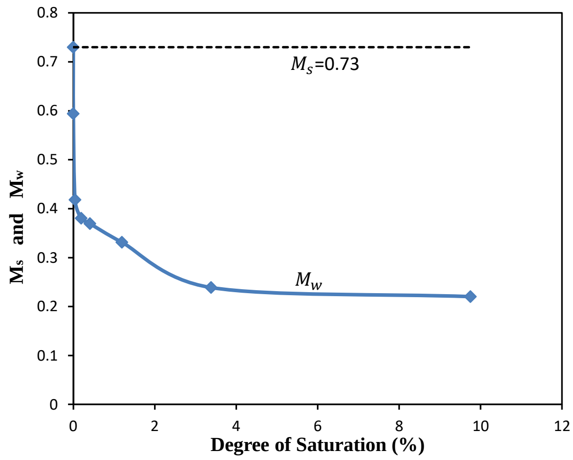

(a) The results from DEM simulations

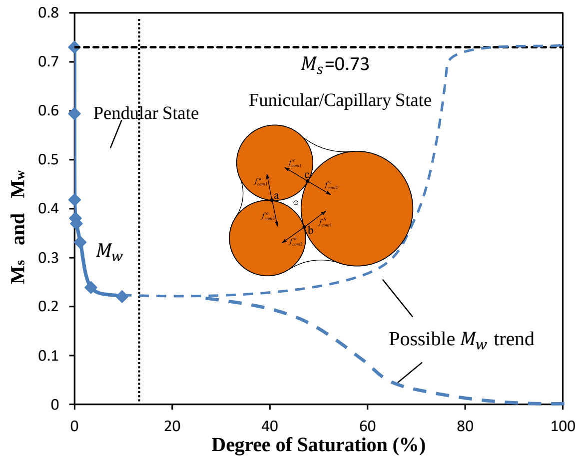

(b) Hypothetical trend beyond the pendular state

Figure 11: The degree of saturation effect on critical state stress ratio parameters.

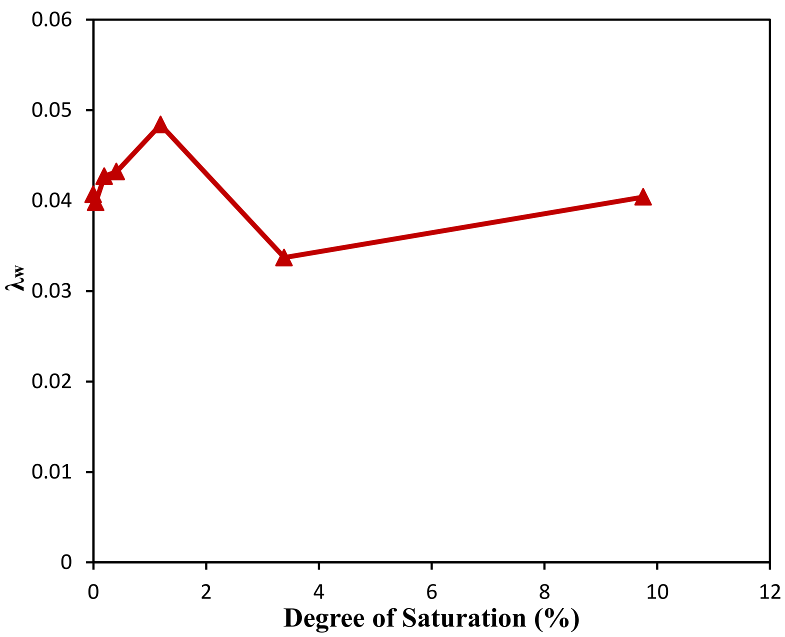

Figure 12: The degree of saturation effect on λ_w.

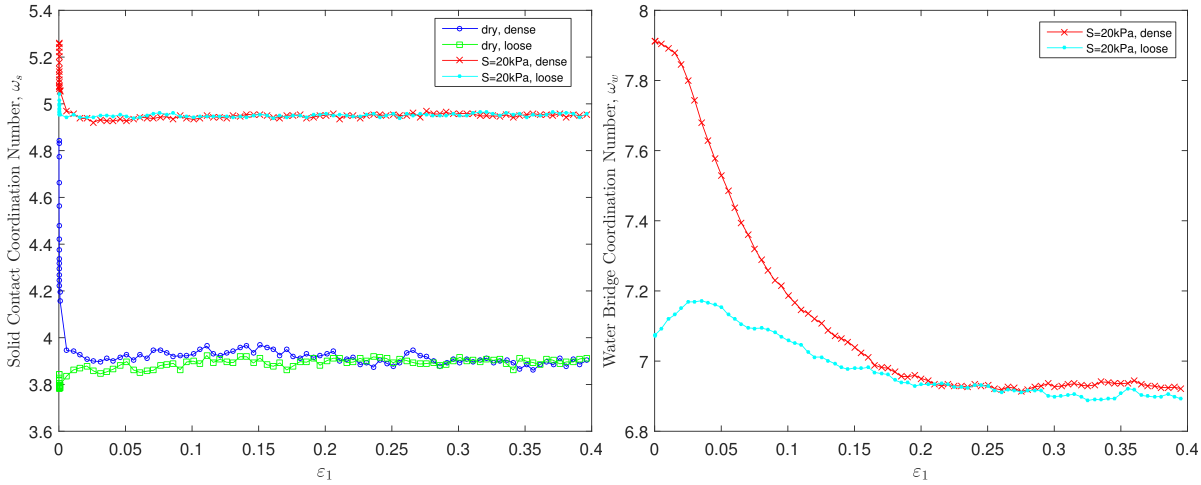

(a) Coordination number of solid contacts (b) Coordination number of water-solid interactions

Figure 13: Evolution of coordination numbers in triaxial shearing.

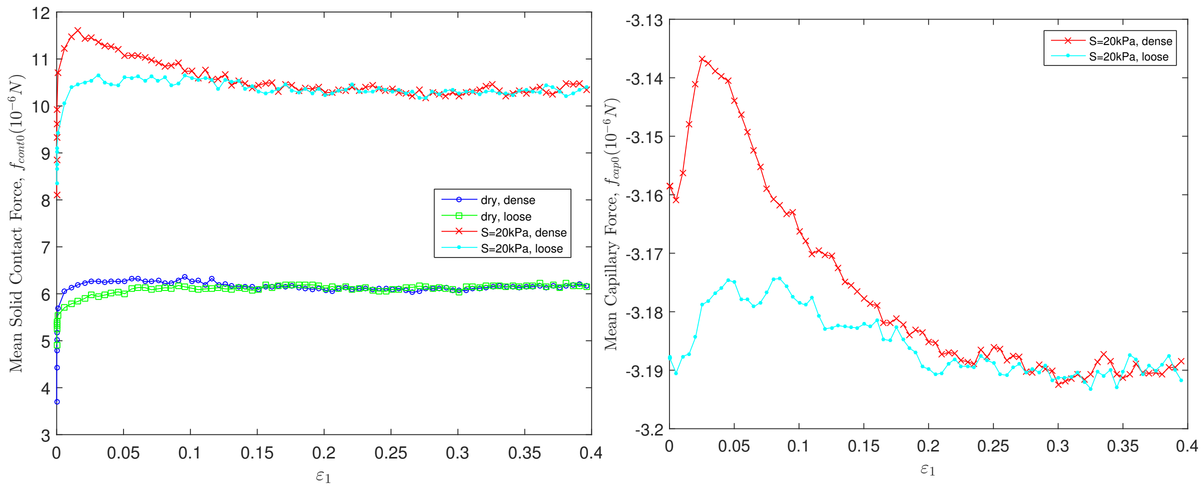

(a) Mean contact forces (b) Mean capillary forces

Figure 14: Evolutions of mean contact and capillary forces in triaxial shearing.

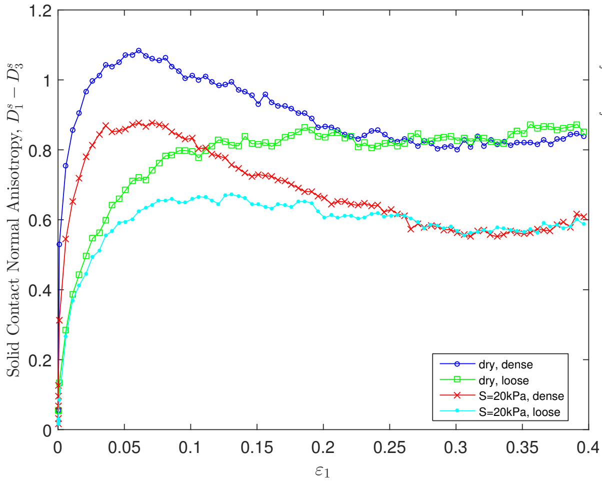

(a) Solid contact fabric anisotropy

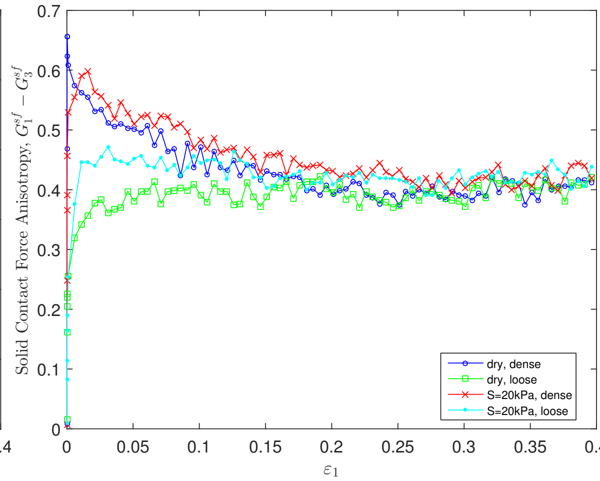

(b) Solid contact force anisotropy

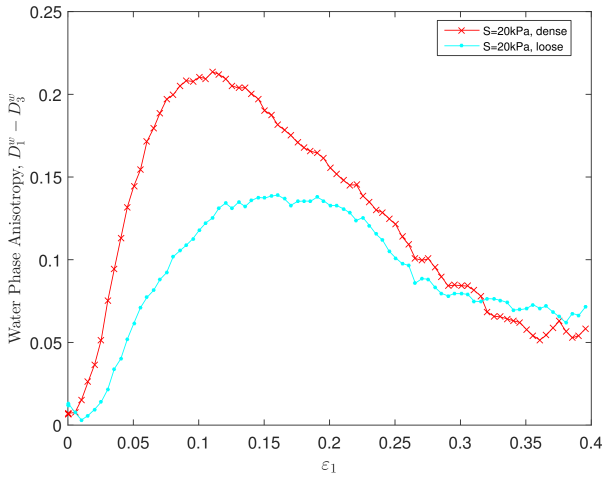

(c) Water bridge network anisotropy

Figure 15: Evolutions of internal fabric and force anisotropies.

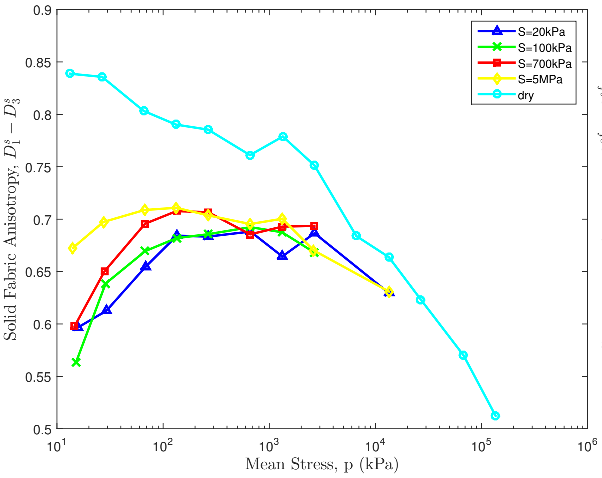

(a) Solid fabric anisotropy

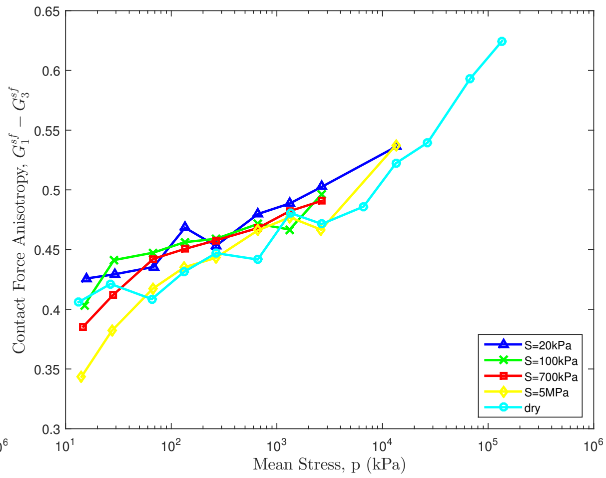

(b) Solid contact force anisotropy

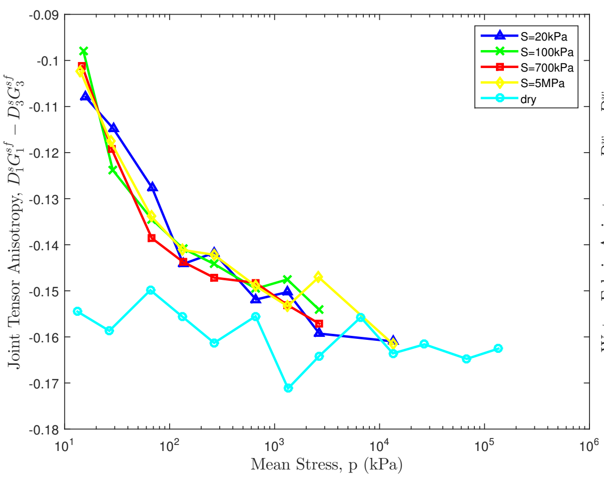

(c) The joint tensor anisotropy

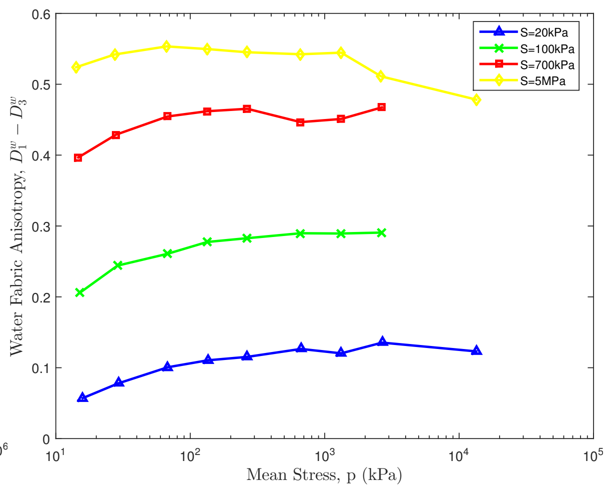

(d) Water fabric anisotropy

Figure 16: The critical state fabric and force anisotropies at different mean stress levels.

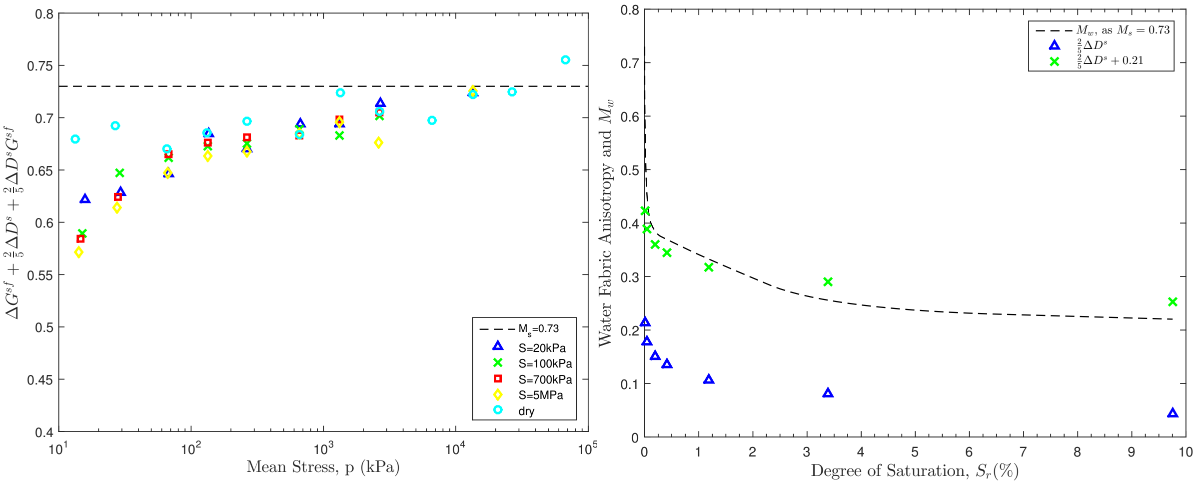

(a) Comparison with parameter M_s

(b) Comparison with parameter M_w

Figure 17: The critical state stress ratio parameters and internal fabric anisotropy.

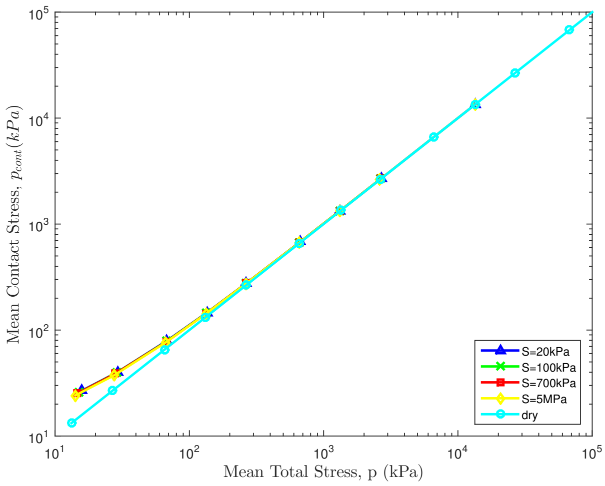

(a) Mean capillary stress

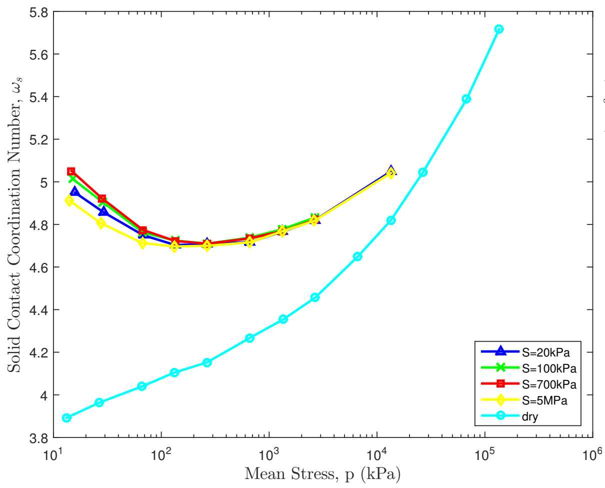

(b) Solid contact coordination number

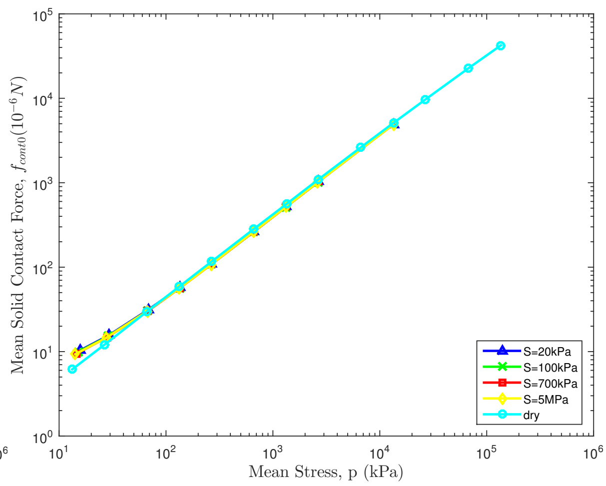

(c) Directional mean contact force

Figure 18: The critical state mean contact stress and its associated micro-parameters at different mean total stress levels.

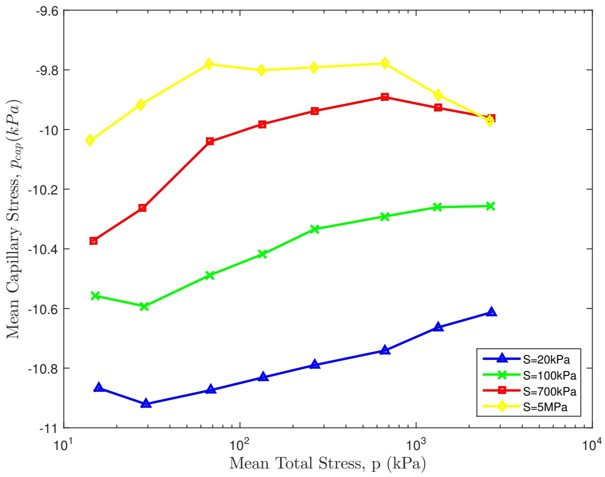

(a) Mean capillary stress

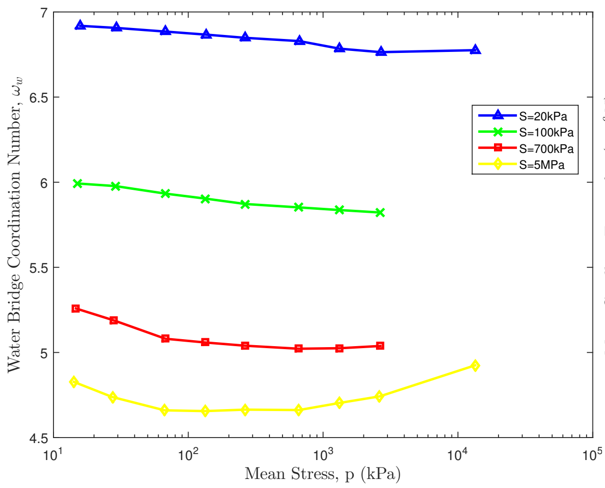

(b) Water bridge coordination number

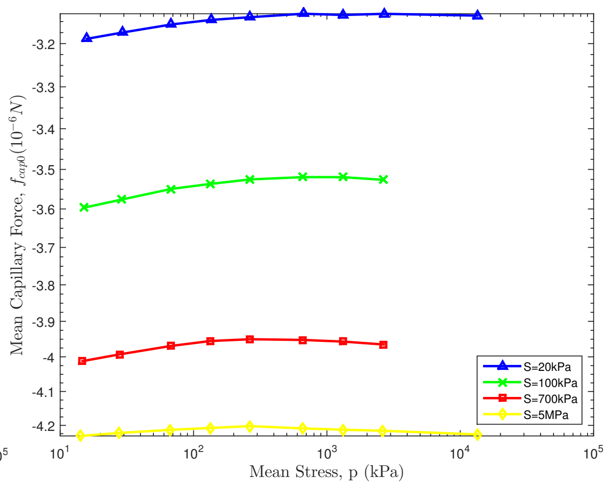

(c) Directional mean contact force

Figure 19: The critical state mean capillary stress and its associated micro-parameters at different mean total stress levels.